Issue no. 1/2006
ECR Edition

MAGNETOM FLASH

www.siemens.com/magnetom-world

Price 10,- EUR

Content

ABDOMEN
Detection of Esophageal Cancer using Body Diffusion Imaging
Page 11

MOLECULAR IMAGING
Iron-Oxide Enhanced Susceptibility-Weighted Imaging of Lymph Node Metastasis
Page 43

NEUROLOGY
Susceptibility-Weighted Imaging (SWI) Case Reports
Page 70

WHOLE-BODY MRI
Faster with Tim
Page 75

SUMMIT
A Glimpse of the Wide Range of Presentations Given at the 4th MAGNETOM World Summit
Page 116 and 125

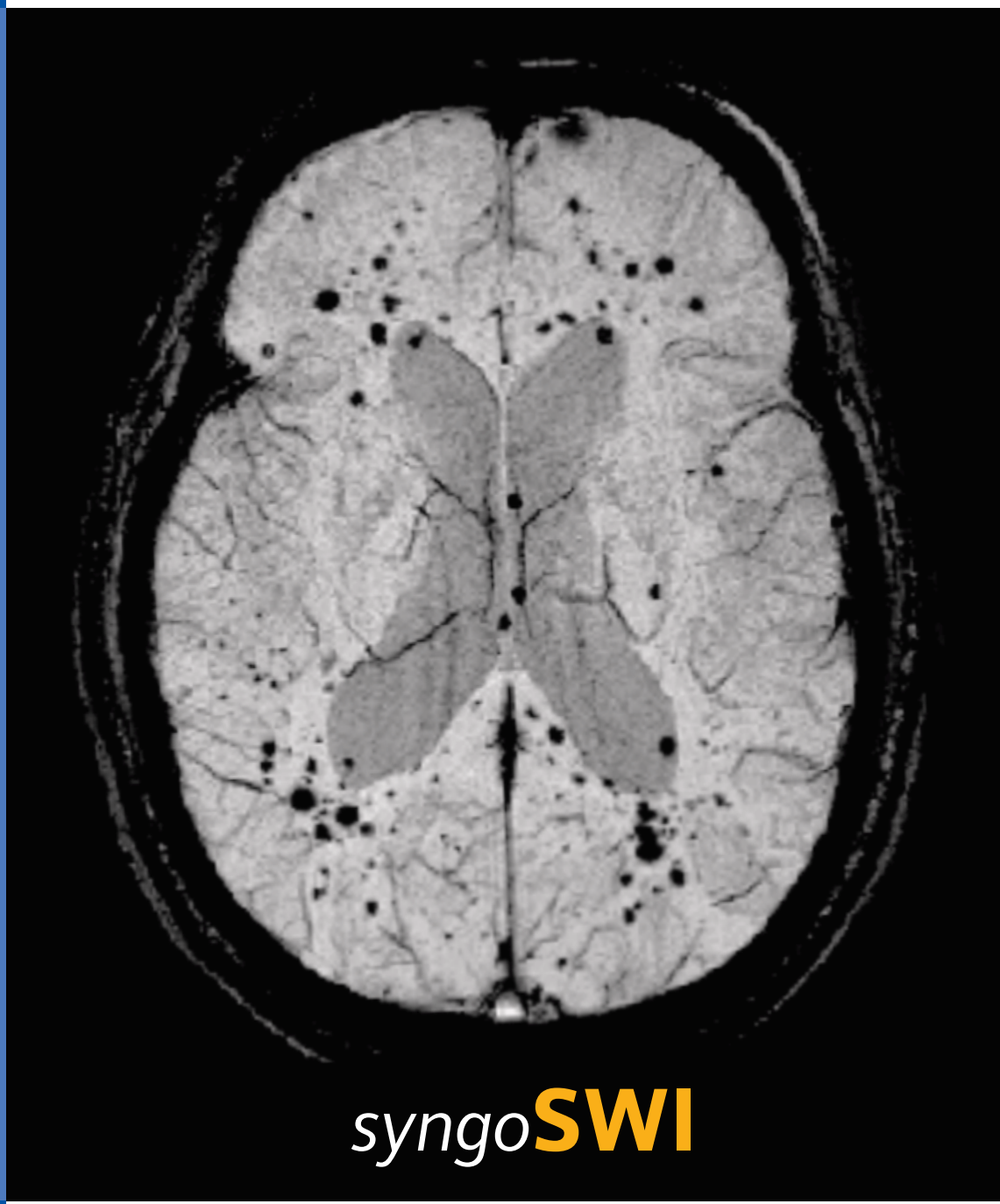

32

SIEMENS
medical

Dear MAGNETOM User,

See More & Work Faster

At this year's RSNA, one of the big hits at the MR booth was SWI (Susceptibility Weighted Imaging). This technique – long TE flow compensated gradient echo imaging providing enhanced contrast with the combination of phase and magnitude information – has provided surprising results in detecting intracranial bleeding and seeing minute intracranial vascular malformations. The verdict was unanimous: "You definitely see more with SWI". Starting on page 70 you will find SWI case reports.

SWI is not a brand new sequence; in fact, it has been around quite a long time. But integrating this sequence within the clinical routine had always been difficult due to long examination times of up to 11 minutes. However, times have changed and today's Tim technology (Total imaging matrix) with GRAPPA Parallel Imaging technique allows this sequence to be run in just 3 to 4 minutes. Whatever the application area – body imaging with VIBE in 12 seconds, whole body imaging in less than 10 minutes, ultra fast dynamic MR Angiography (MRA) or new sequences like SWI – you always work faster with Tim and GRAPPA.

The 2005 MAGNETOM World Summit came to Singapore. The images on pages 116 ff. and a short summary of some of the presentations will offer you a taste of a very successful Summit, with attendance numbers of 350 MAGNETOM users and an unsurpassed number of presentations covering almost every area in MR, including molecular imaging.

But don't worry if you have missed it, the 5th MAGNETOM World Summit in San Diego, California, USA is just around the corner. Between June 8 and June 11, 2006 you'll find an excellent platform to establish personal contacts, exchange valuable information, learn from the experience of other users and to share your own expertise. For a glance at the agenda and registration please visit us at www.siemens.com/magnetom-world.

Enjoy reading MAGNETOM Flash

A. Nejat Bengi

MAGNETOM Flash is part of Life, Siemens' unique customer care solution that helps you get the most from your investment. With its programs and services Life sharpens your skills so you can see optimal clinical value. It provides the support you need to maximize productivity and it assures that as technology changes, you will always be at the cutting edge. Life. You can count on it.

The Editorial Team

We appreciate your comments.
Please contact us at magnetomworld.med@siemens.com

Lisa Reid,
US Installed Base Manager,
Malvern, PA

Dagmar Thomsik-Schröpfer, Ph.D.
MR Marketing-Products, Erlangen

Antje Hellwich
Associate Editor

A. Nejat Bengi, M.D.
Editor in Chief

Heike Weh,
Clinical Data Manager,
Erlangen

Bernhard Baden,
Clinical Data Manager,
Erlangen

Tony Enright, Ph.D.
Asia Pacific Collaborations,
Australia

Milind Dhamankar, M.D.
Manager Clinical MR
Research Collaborations,
Siemens Medical
Solutions USA

Peter Kreisler, Ph.D.
Collaborations & Applications,
Erlangen

Gary R. McNeal, MS (BME)
Advanced Application Specialist,
Cardiovascular MR Imaging
Siemens Medical Solutions USA

Cécile Mohr, Ph.D
Head of Market Segment
Management, Erlangen

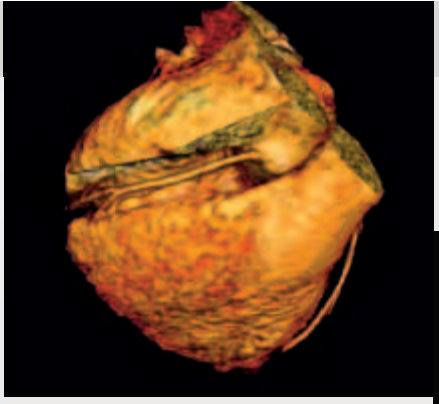

Coronary MRA. ***Page 19***

Interventional MRI. ***Page 39***

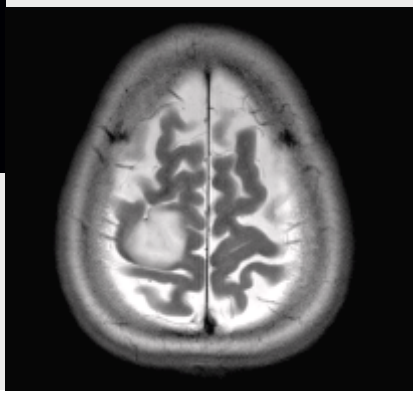

7 **PRODUCT NEWS**
Blade. For Clear-Cut Imaging

CLINICAL

10 **ABDOMEN AND PELVIS**
Early Gastric Cancer Diagnosis using Body Diffusion Imaging

11 **ABDOMEN AND PELVIS**
Detection of Esophageal Cancer Using Body Diffusion Imaging

12 **ABDOMEN AND PELVIS**
Case Report MAGNETOM Avanto Complicated Rectal Fistula

13 **ABDOMEN AND PELVIS**
Case Report MAGNETOM Avanto Recurrent Rectal Cancer Evaluation with VIBE and SPACE

16 **CARDIAC**
Whole Heart MRI – Adopting the CT Approach

24 **HEAD AND NECK**
Non-EPI Diffusion-Weighted MR Imaging in the Diagnosis of Cholesteatoma

30 **HEAD AND NECK**
The Utility of Surface Coils and New Sequences in Orbital and Ocular MR Imaging

36 **HEAD AND NECK**
Differentiating Primary Parotid Gland Lesions by Diffusion-Weighted MR Imaging

38 **INTERVENTIONAL**
3T Ultra High-Field Intraoperative MR with Twin Room Concept

43 **MOLECULAR IMAGING**
Iron-Oxide Enhanced Susceptibility-Weighted Imaging of Lymph Node Metastasis

46 **MOLECULAR IMAGING**
Intravenous Cellular MR Contrast Agent with a Great Clinical Potential

52 **NEUROLOGY**
Use of Turbo GRAPPA IR Imaging in Parkinson's Disease

57 **NEUROLOGY**
The Neuro3D Task Card

62 **NEUROLOGY**
Functional High-Resolution 3D Examinations of the Cervical Spine with Magnetic Resonance Imaging

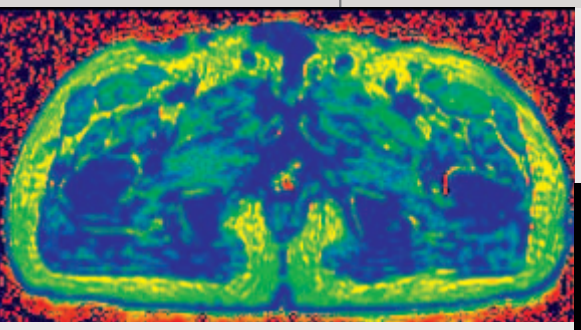

T2 maps in diagnosis of lymph node metastasis.* ***Page 44***

Perioperative use of DTI. ***Page 40***

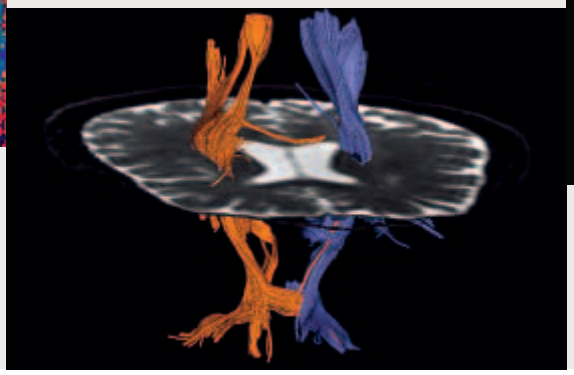

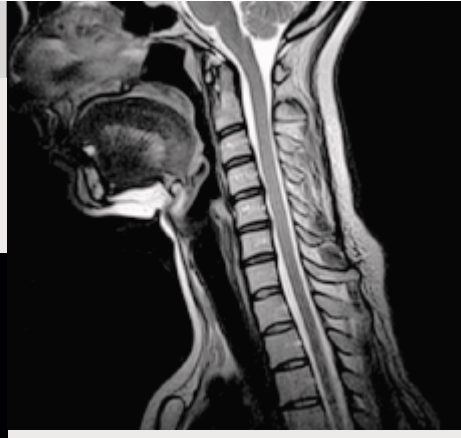

MAGNETOM C! Cervical spine. ***Page 118***

70 **NEUROLOGY**
Susceptibility-Weighted Imaging (SWI) Case Reports

75 **WHOLE-BODY MRI**
Whole-Body MRI: Faster with Tim

81 **WOMEN'S HEALTH**
High-Resolution Dynamic Breast MRI. Current Capabilities of *syngo* MR MAGNETOM Systems

86 **WOMEN'S HEALTH**
integrated Parallel Acquisition Techniques (iPAT) in Breast MRI

91 **WOMEN'S HEALTH**
Combination of a Large Loop Flex Coil with the Breast Coil Improves Evalutation of the Lymph Nodes in the Auxiliary and Pectoral Region

94 **WOMEN'S HEALTH**
^{1}H MR Spectroscopy of the Breast at 1.5T and 3T

TECHNOLOGY

98 **AUTOALIGN**
Software Compensation for Patient Position Enabling Reproducible Slice Position

104 **CLOVERLEAF**
Structural MR Imaging with Real-Time Prospective Rigid Body Motion Correction using Cloverleaf Navigators

108 **HELIUM**
Hyperpolarized Helium Magnetic Resonance Lung Imaging

LIFE

116 **SUMMIT**
A Glimpse of the Wide Range of Presentations Given at the 4th MAGNETOM World Summit

125 **SINGAPORE**
Looking back at the 4th MAGNETOM World Summit in Singapore

132 **IMPRINT**

The information presented in MAGNETOM Flash is for illustration only and is not intended to be relied upon by the reader for instruction as to the practice of medicine. Any health care practitioner reading this information is reminded that they must use their own learning, training and expertise in dealing with their individual patients. This material does not substitute for that duty and is not intended by Siemens Medical Solutions to be used for any purpose in that regard. The drugs and doses mentioned in MAGNETOM Flash are consistent with the approval labeling for uses and/or indications of the drug. The treating physician bears the sole responsibility for the diagnosis and treatment of patients, including drugs and doses prescribed in connection with such use. The Operating Instructions must always be strictly followed when operating the MR System. The source for the technical data is the corresponding data sheets.

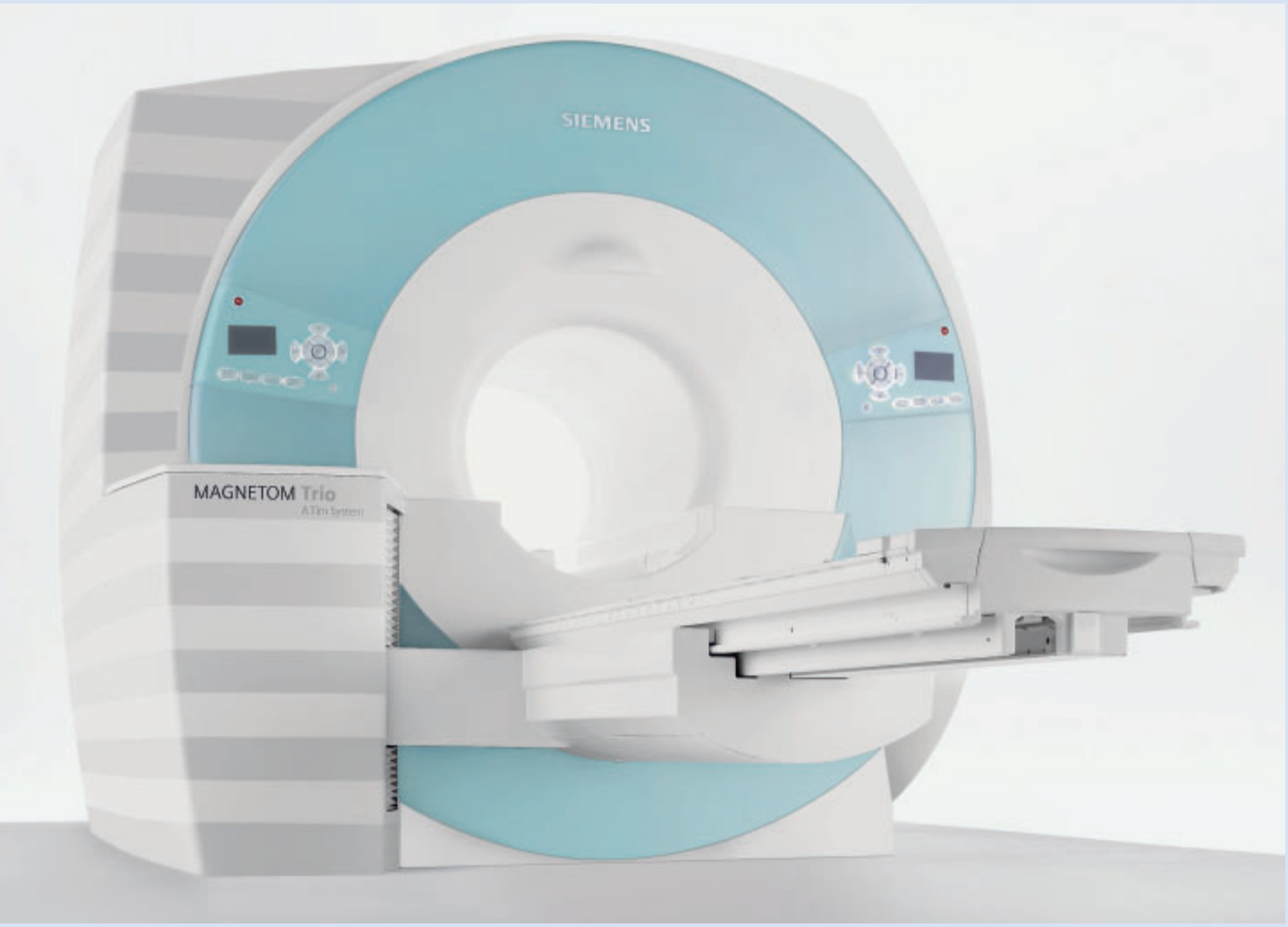
SIEMENS
MAGNETOM Trio

SIEMENS

BLADE – For Clear-Cut Imaging

Innovation for every day use

BLADE is a technique that incorporates a k-space trajectory radial in nature and a motion correction which reduces dramatically sensitivity to movement. BLADE works fully automatically.

BLADE eliminates repeats

BLADE ensures that you get the best results all the time, from the youngest to the oldest patients, without having to worry if the images will be good enough. With BLADE, you can confidently acquire the data and make the diagnosis. No need to repeat the measurement and no need to recall the patient to rescan.

BLADE reduces the sedation rate

With BLADE's low sensitivity to motion, you can now start thinking about reducing sedation rate in pediatric or anxious patients. And this is not only good for your patient but also increases your time-efficiency.

BLADE for all contrasts and all orientations

BLADE supports your workflow. Whatever orientation – axial, sagittal or coronal – or contrast – T1, T2 and Dark Fluid – you need.

BLADE is coil-independent

BLADE works with Tim coils, the multi-channel Matrix coils such as the 12-channel Head Matrix, the 16-channel Head-Neck Matrix combination, dedicated array coils, as well as accessory coils.

BLADE at all field strengths

Discover BLADE on Tim Upgrades and all Tim systems – at 1.5T MAGNETOM Avanto, Espree, Symphony and at 3T MAGNETOM Trio.

BLADE – All contrasts, all orientations

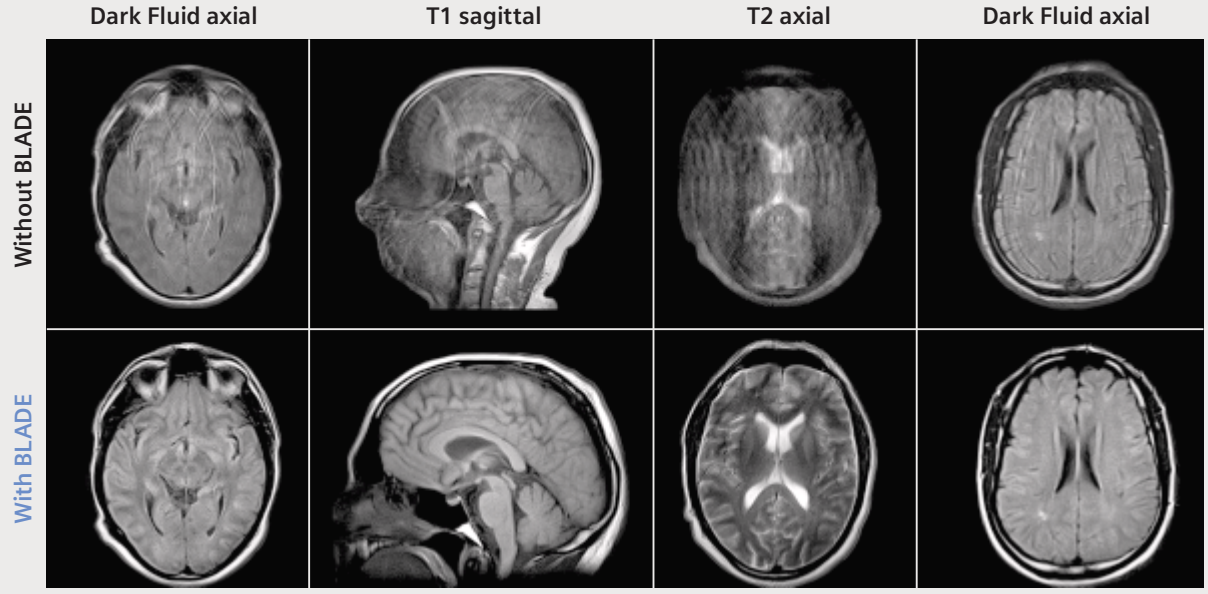

MAGNETOM Trio and MAGNETOM Espree with Tim.

Courtesy of Klinikum Bremen Mitte, Germany and Mayo Clinic, Jacksonville, Florida, USA

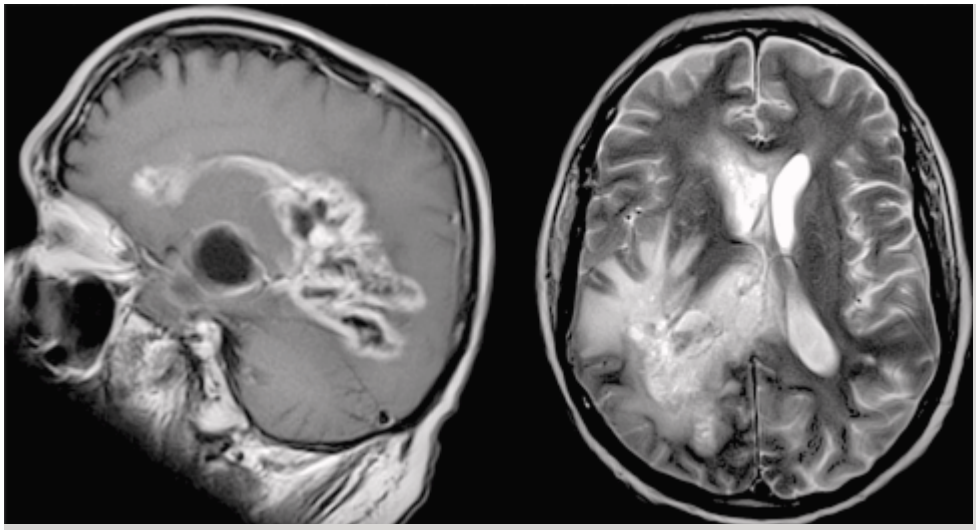

Tumor
MAGNETOM Avanto 12-channel Head Matrix. T1 sagittal post contrast with BLADE.
Courtesy of Northwestern Memorial Hospital, Chicago, USA

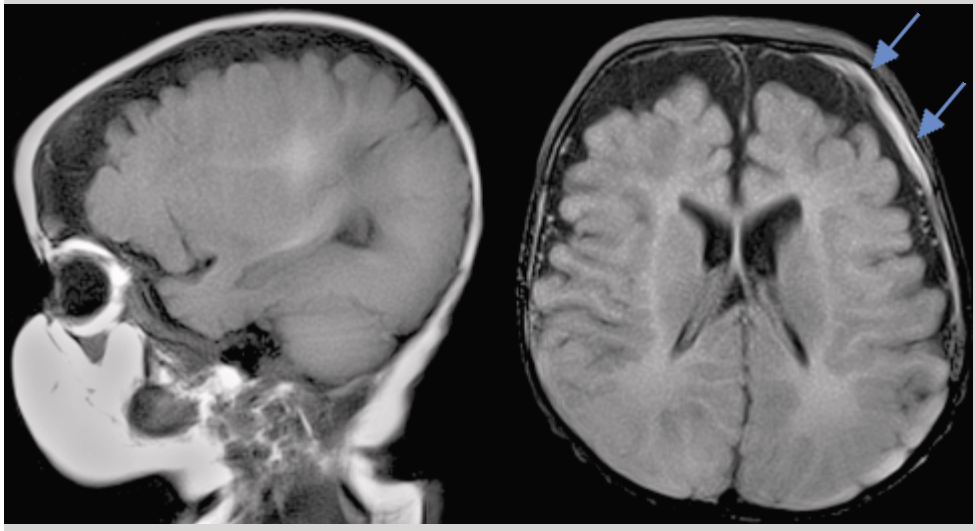

Pediatric imaging. Left fronto-temporal subdural hematoma. Non-sedated child 3-month-old. MAGNETOM Avanto 12-channel Head Matrix. T1 sagittal with BLADE Dark Fluid axial with BLADE.
Courtesy of Children's Hospital of Philadelphia, USA

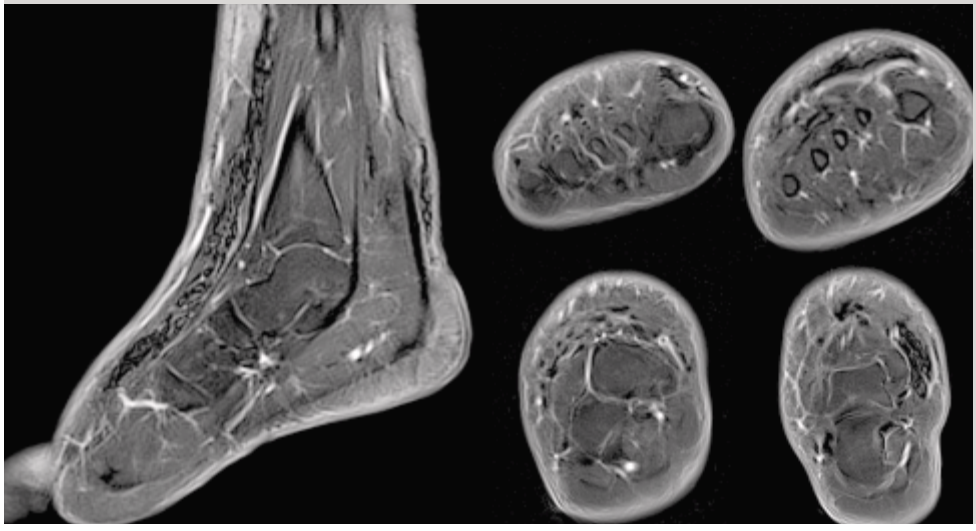

Orthopedic imaging with fat suppression in the bone marrow of a 15-year-old child. MAGNETOM Avanto 12-channel Head Matrix. T2 TIRM sagittal and axial with BLADE.
Courtesy of Children's Hospital of Philadelphia, USA

Abdomen and Pelvis

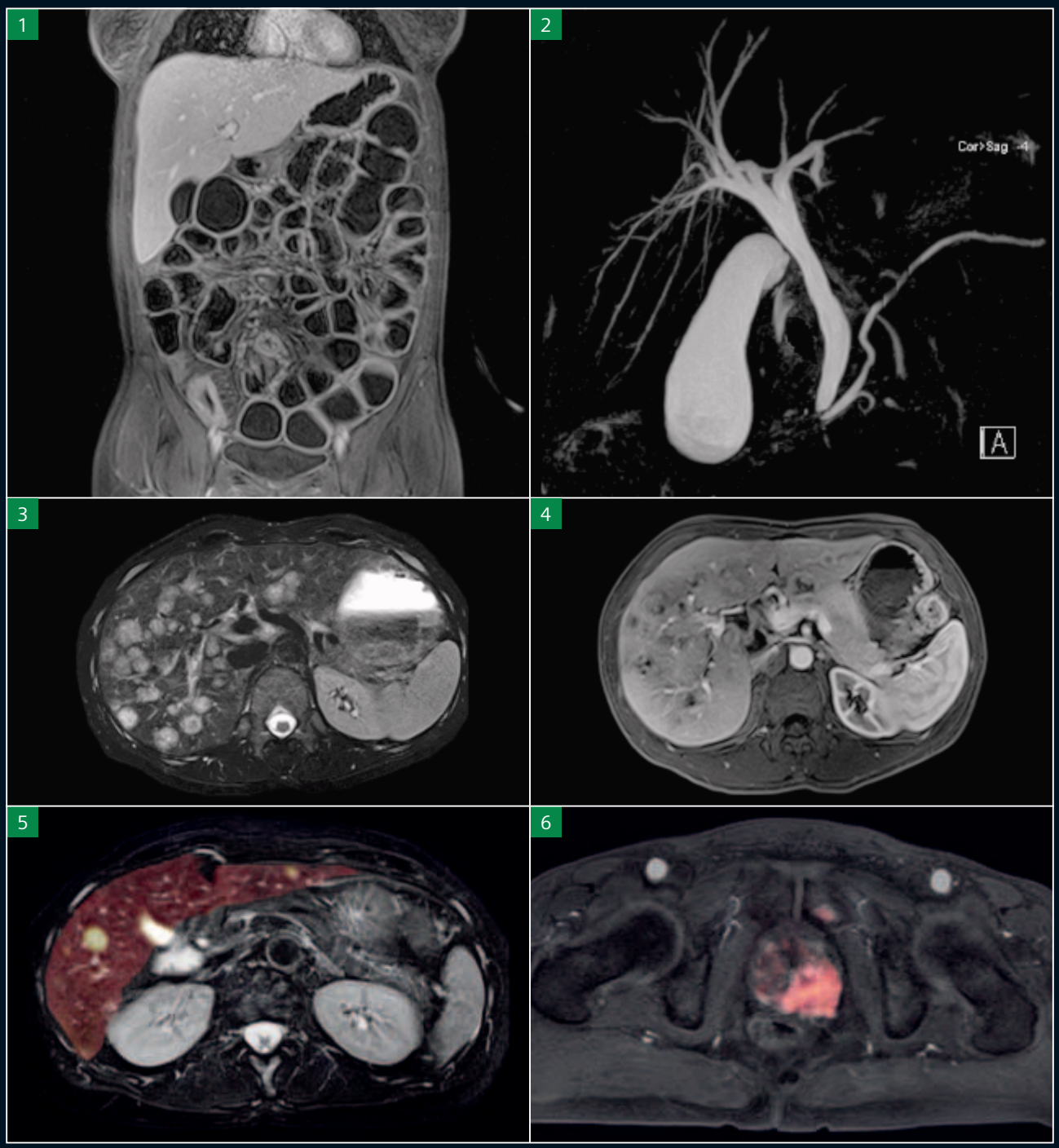

[1, 3, 4, 5] Courtesy of LMU Grosshadern, Munich, Germany
[2] Courtesy of St. Vincent's Melbourne, Melbourne, Australia
[6] Courtesy of Gunma Cancer Center, Gunma, Japan

Early Gastric Cancer Diagnosis using Body Diffusion Imaging

Noriatsu Ichiba, M.D.

Tokyo Jikei University School of Medicine, Tokyo, Japan

Patient history

55-year-old male; chief complaint was epigastralgia.

Sequence details

Respiratory triggered diffusion-weighted imaging (DWI) with PACE (Prospective Acquisition CorrEction). Axial scan, CHESS pulse, TR 1400, TE 64, Bandwidth 2368, Averaging 5, GRAPPA factor 2, b = 50 and b = 800, FOV 500 mm, Matrix 192, slice thickness 7 mm, number of slices 32, respiratory triggering with PACE.

Results

There was no remarkable abnormality on the T1-weighted image (Fig.1), the T2-weighted image (Fig. 2) and early phase (Fig. 3) and delayed phase (Fig. 4) of contrast enhanced dynamic MRI.

There was a flat membranous lesion on gastric lesser curvature with slightly high signal on low b-value DWI (b = 50, Fig. 5) and high b-value DWI (b = 800, Fig. 6). This finding was suggestive of early gastric cancer, corresponding with endoscopic finding. Additionally, a small lymph node showed high signal on DWI, suggestive of metastasis.

Discussion

Early gastric cancer was detected with diffusion-weighted imaging (DWI). With use of antiperistalsis agents, the detectability of membranous lesion may improve on DWI.

Scanner	*MAGNETOM Avanto 1.5T with SQ-engine*
Coils	*Body Matrix Coil, Spine Matrix Coil*
Software version /add-on	*syngo MR 2004V / Work-in-progress sequence**

*This information about this product is preliminary. The product is under development and not commercially available in the US and its future availability cannot be ensured.

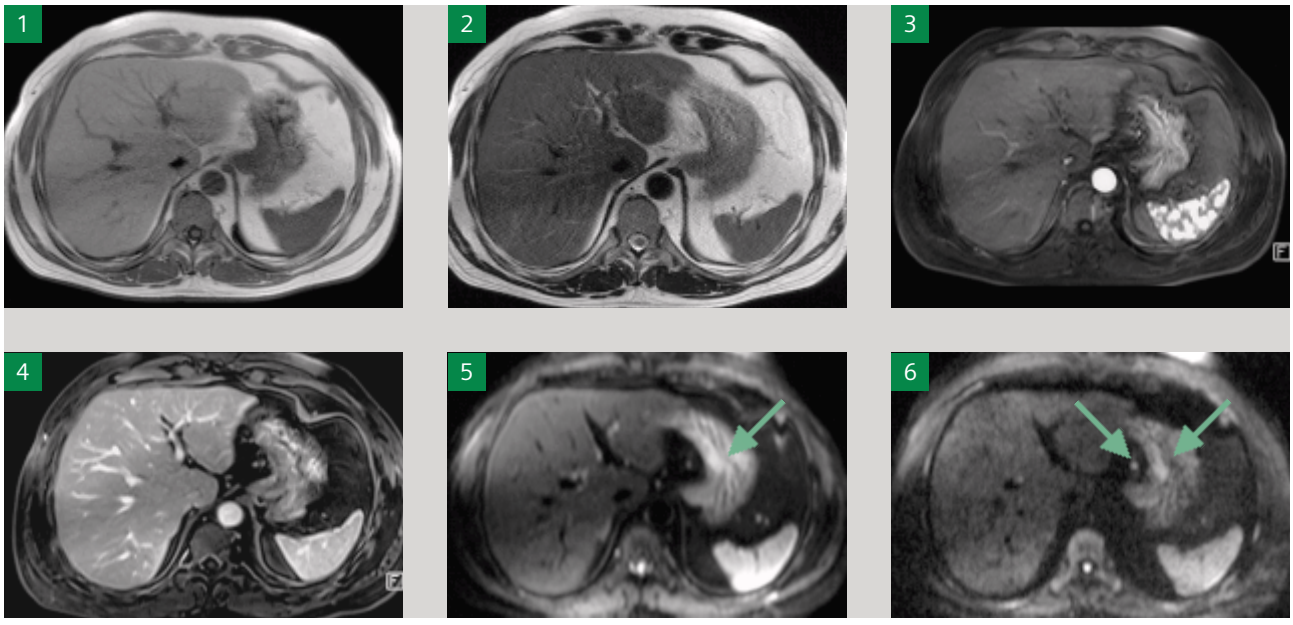

Detection of Esophageal Cancer Using Body Diffusion Imaging

Takashi Koyama, M.D., Ph.D.

Dept. of Radiology, Kyoto University Hospital, Kyoto, Japan

Patient history

A 65-year-old asymptomatic man who was diagnosed with esophageal cancer of T1b stage (with invasion into the submucosal layer) during a routine endoscopy examination. The patient was referred for an MR examination.

Sequence details

Initially, T2-weighted fast Spin Echo images were obtained for defining anatomy and localizing the tumor. The location of the esophageal tumor was estimated by rough clinical information. Following T2-weighted imaging (T2WI) with sagittal or oblique sagittal plane along the course of the esophagus, diffusion-weighted imaging (DWI) with same plane was obtained utilizing a single shot echo-planar sequence with respiratory-triggering. Parameters for DWI included TR of 4000 ms, TE of 74 ms, b factors of 0 and 500 (s/mm^2), PAT factor of 2 using GRAPPA (PAT = Parallel Acquisition Technique), length of echo train (EPI factor) of 110, bandwidth of 1346 Hz/pixel, matrix of 128 x 128, and number of acquisition of 5. Both T2-weighted and diffusion-weighted images were uniformed with a section thickness of 3 mm without intersection gap, and a field of view of 350 mm.

Results

We have investigated the difference in detectability of esophageal cancer between diffusion-weighted images and T2-weighted images. Our study population included pathologically proven 13 patients with age ranging from 47 to 74 years old (mean: 62). The histologic diagnosis of the tumor was squamous cell carcinoma in all patients. The pathologic stage of esophageal cancer in 13 patients who were surgically treated were T3 (n=7), T2 (n=2) and T1b (n=4). T2-weighted images failed to demonstrate four T1b cancers, whereas fusion images with T1b and T2-weighted images failed to demonstrate only one T1b cancer.

Discussion

MRI has achieved limited clinical use in the evaluation of esophageal cancer. Reasons for this include the substantial artifacts from breathing and cardiac motion, long examination times, and as a result, poor imaging quality and reliability. Our study shows that DWI with respiratory-triggering can successfully demonstrate esophageal cancer as high intensity lesions in a majority of the patients. One of the big advantages of DWI over ordinary MR images is that this technique can demonstrate esophageal cancers with excellent tissue contrast, whereas T2WI demonstrates mere wall thickening of the esophagus. Even the esophageal cancers with T1b stage, which are confined within submucosal layer of the esophagus, can be demonstrated on DWI, whereas these tumors are generally hardly recognized on ordinary T2WI. The excellent tissue contrast on DWI may be explained by the difference of water diffusion between the cancer and normal esophagus. In the esophageal cancers, movement of water molecules may be restricted due to the increased cellularity and nuclear to cytoplasmic ratio.

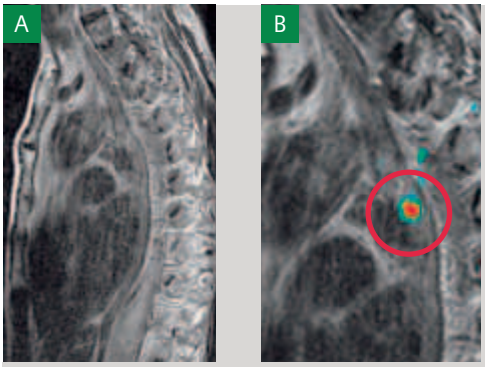

[A] *Free-breathing T2WI with PACE (Prospective Acquisition CorrEction) hardly shows any abnormality in the esophagus.*
[B] *Fusion image of DWI onto T2WI shows a focal area of increased signal intensity in the upper thoracic esophagus. The lesion was confirmed to be esophageal cancer of T1b stage at surgery.*

Scanner	*MAGNETOM Symphony*
Coils	*CP Body Array Coil, CP Spine Array Coil*

Case Report MAGNETOM Avanto
Complicated Rectal Fistula

Arnd-Oliver Schäfer, M.D.

University Hospital Freiburg, Department of Radiology, Freiburg, Germany

Patient history

38-year-old man with gluteal abscess had undergone incision. Delayed healing and persistent secretion gave rise to the suspicion of an underlying fistula. Subtraction MR-Fistulography was performed to exclude the suspected diagnosis.

Image findings

At coronal TIRM sequence high signal intensity abscess is shown within the left gluteus muscle (Fig. 1A) which communicates with a fluid-filled formation above the level of the levator muscle surrounding the lower rectum (Fig. 1B). Note

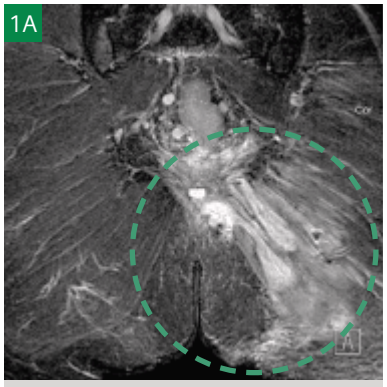

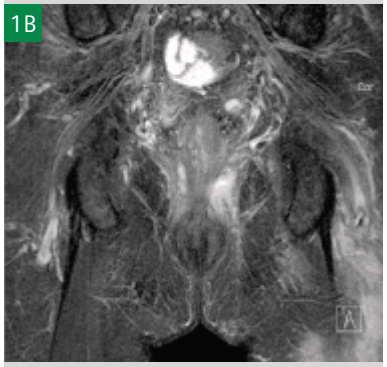

[Figure 1] *Coronal Turbo Inversion Recovery Magnitude –TIRM.*

TI	*150 ms*
TR	*5289 ms*
TE	*60 ms*
slice thickness	*3 mm*
matrix	*512 x 512*
FoV	*250 mm*
flip angle	*150°*
BW	*130 Hz/Px.*

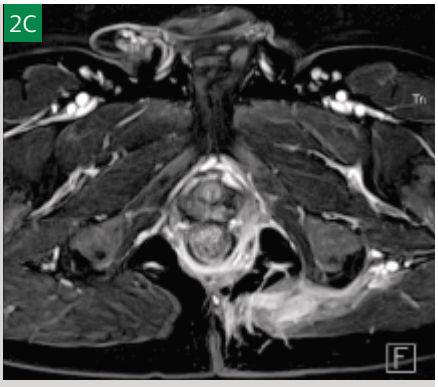

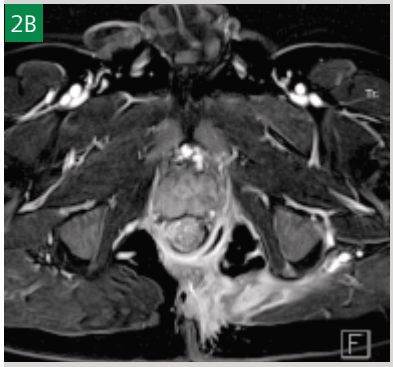

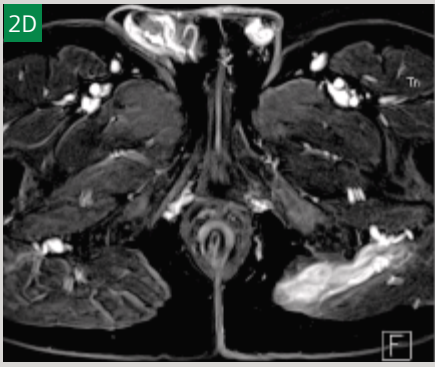

[Figure 2] *Axial Fast Low Angle Shot-3D – 3D FLASH*

TR	*7 ms*
TE	*2.7 ms*
slice thickness	*2 mm*
matrix	*512x 256*
FoV	*250 mm*
flip angle	*45°*
BW	*130 Hz/Px.*

also the reactive lymph nodes inside the mesorectum (Fig. 1A). On the axial contrast-enhanced 3D FLASH sequence after image subtraction a rectal fistula is clearly delimitable, forming a supralevatoric horseshoe (Fig. 2A). The internal opening is located at 9 o'clock lithotomy position. The fistula passes the levator muscle at 4 o'clock (Fig. 2B) towards the fat of the left-sided ischiorectal fossa. The fistula retains pus and is directly connected to the residual gluteal abscess (Figs. 2C, D). MIP-reconstruction of the data derived from the 3D FLASH sequence is giving a survey of the whole extent of inflammation (Fig. 3).

Discussion

To detect and precisely assess the extent of anorectal fistulas subtraction, MR-fistulography is extremely helpful. Contrast-agent based, gradient-echo imaging provide excellent anatomic resolution and the capability to perform image reconstructions on the one hand as well as thin-sections and high sensitivity for inflammation on the other hand.

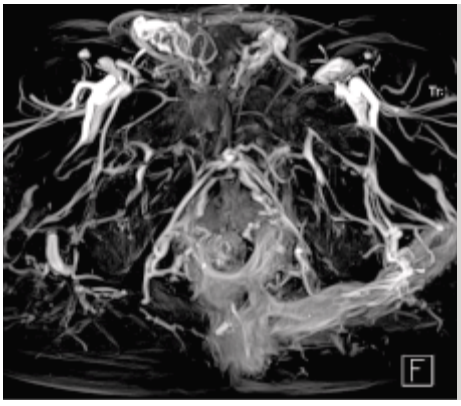

[Figure 3] *3D FLASH, Maximum Intensity Projection (MIP) reconstruction.*

Case Report MAGNETOM Avanto
Recurrent Rectal Cancer Evaluation with VIBE and SPACE

Arnd-Oliver Schäfer, M.D.

University Hospital Freiburg, Department of Radiology, Freiburg, Germany

Patient history

48-year-old woman with cancer of the lower rectum received transanal endoscopic microsurgery (TEM) in 2003. In that year a recto-vaginal fistula was also closed. Currently, the patient presented with perianal pain and recurrent rectal cancer was diagnosed. Pelvic MRI was performed to determine the extent of the recurrent tumor.

Image findings

A sagittal T2-TSE sequence demonstrates the recurrent rectal cancer located above the anal canal infiltrating the right-sided levator muscle (Figs. 1A, B, C). Additionally, fluid is accumulated in the vaginal lumen after rectal water filling indicating ano-vaginal fistula. On the axial T2 SPACE sequence (Figs. 2A, B, C) and the corresponding axial contrast-enhanced VIBE sequence (Figs. 3A, B, C) the tumor is infiltrating the mesorectal fat, the mosrectal fascia and the parietal peritoneal fascia along a scar formation on the right side with small amounts of ascites indicative for peritoneal spread (Fig. 2A). Infiltration of the right levator muscle is seen (Figs. 2, 3). There are no lymph nodes present.

Discussion

Pelvic anatomy can be imaged exquisitely with the 3D, high-resolution T2 SPACE sequence as well as with the high-resolution contrast-enhanced T1 VIBE sequence. A combination of both appears to be useful particularly for local staging of rectal cancer.

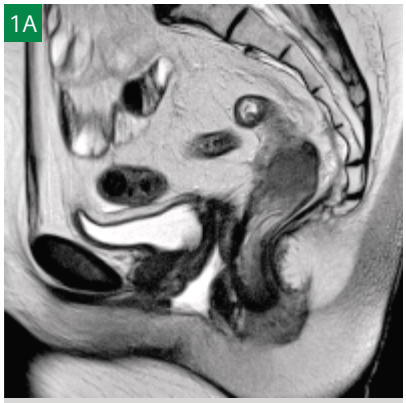

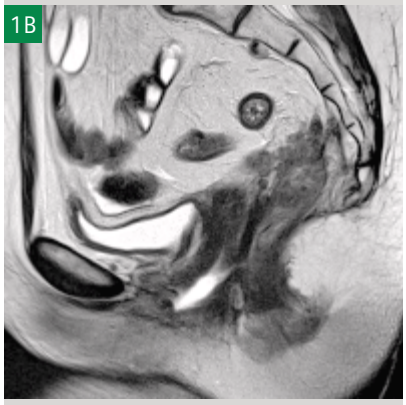

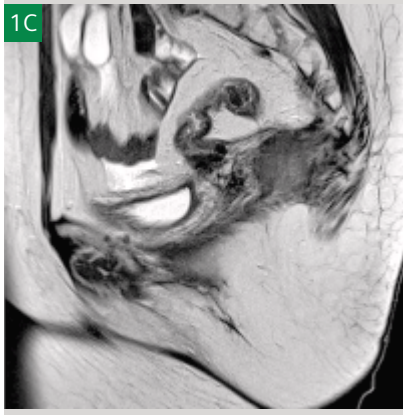

[Figure 1] *Sagittal T2-weighted Turbo Spin Echo –TSE.*

TR	*4960 ms*
TE	*126 ms*
slice thickness	*6 mm*
matrix	*512 x 256*
FoV	*280 mm*
flip angle	*150°*
BW	*195 Hz/Px.*

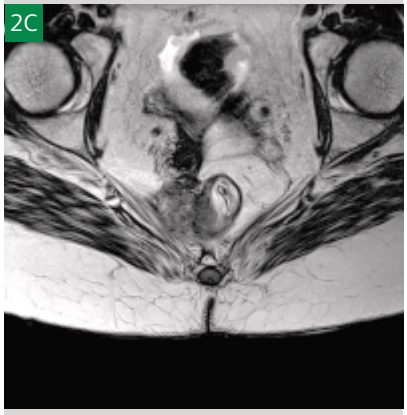

[Figure 2] *Axial T2 SPACE (Sampling Perfection with Application optimized Contrasts using different flip angle Evolutions).*

TR	*1500 ms*
TE	*166 ms*
slice thickness	*2 mm*
matrix	*512 x 256*
FoV	*250 mm*
flip angle	*150°*
BW	*444 Hz/Px.*
iPAT	*PAT 2, GRAPPA.Hz/Px.*

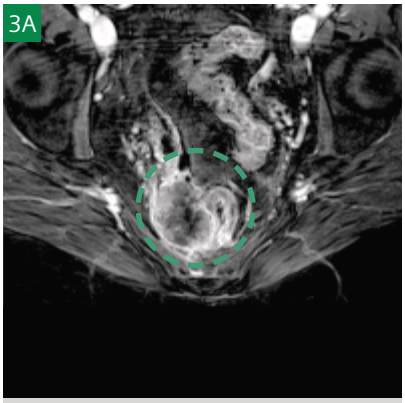

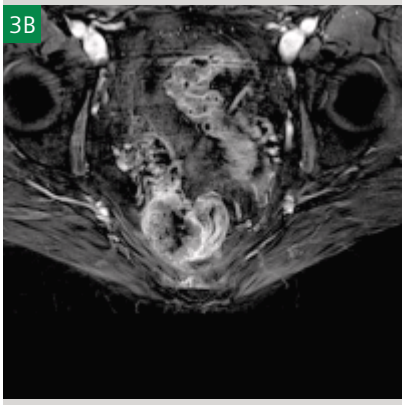

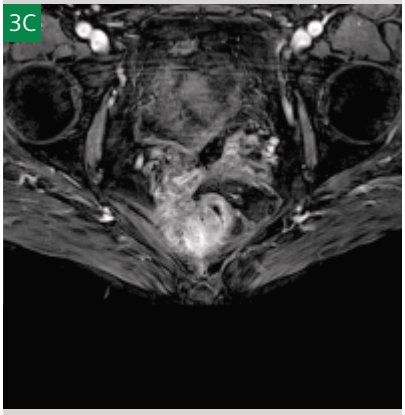

[Figure 3] *Axial Volume Interpolated Breathhold Examination – VIBE.*

TR	*8.30 ms*
TE	*3.23 ms*
slice thickness	*2.5 mm*
matrix	*512 x 256*
FoV	*250 mm*
flip angle	*125°*
BW	*150 Hz/Px.*

Cardiac

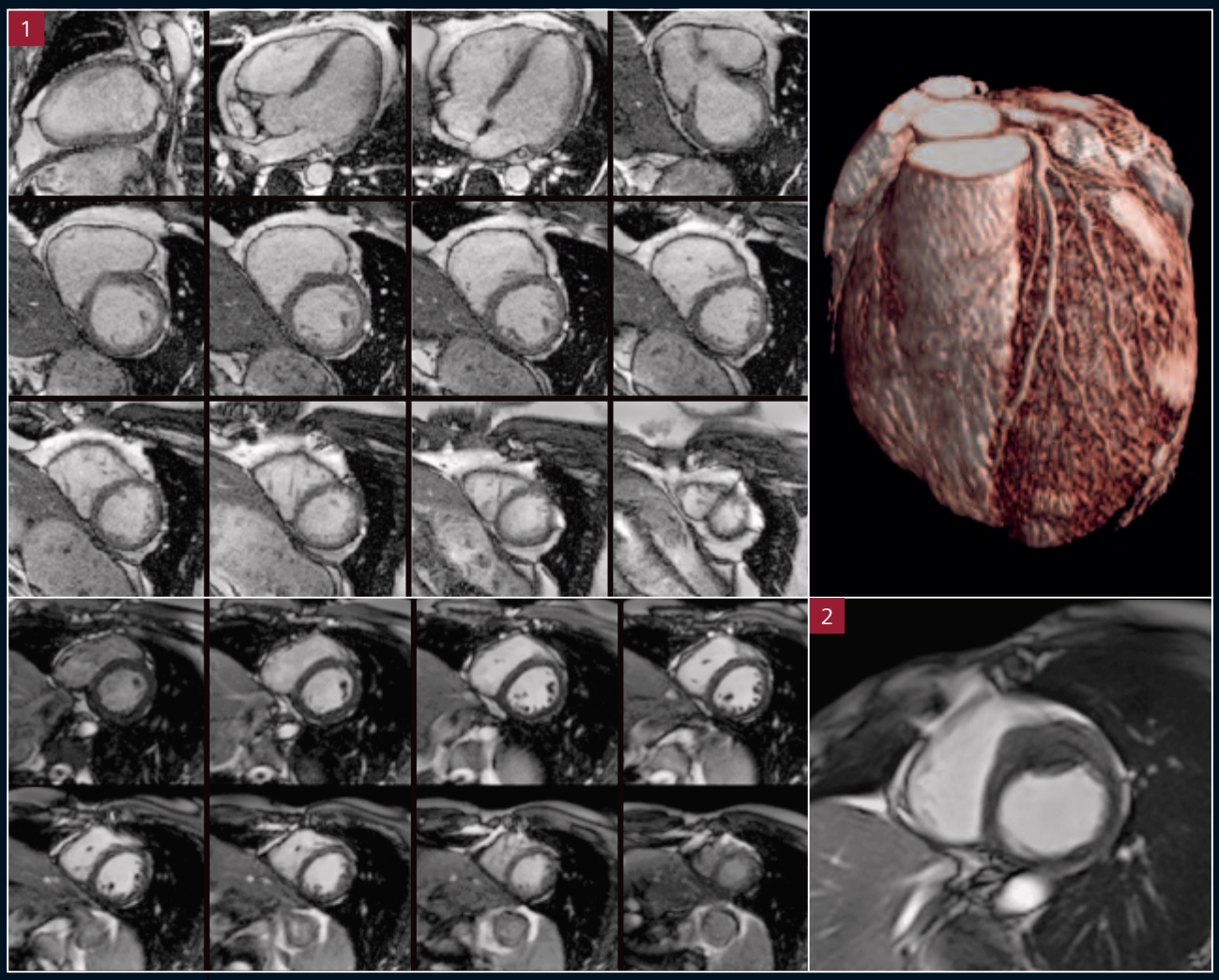

[1] Courtesy of P. Kellman, NHLBI, NIH, Bethesda, USA
[2] Courtesy of Dr. K. Teraoka, Tokyo Medical Univ., Japan

Whole Heart MRI – Adopting the CT Approach
3D Coronary Tree & Cardiac Morphology

Gary R. McNeal

MS (BME), Siemens Medical Solutions Inc., USA

Cardiovascular MR (CMR) is already established as a non-invasive technique for the assessment of coronary artery disease looking at heart function, morphology and tissue characterization. CMR therefore provides valuable information about the tissue damage caused by coronary artery stenosis, e.g showing the distribution of myocardial scar at the subendocardial level. The non-invasive visualization of the coronary arteries themselves is currently a domain of cardiac CT, which provides excellent images of the whole heart within 10–15 s with an isotropic resolution below 0.5 mm. With Tim

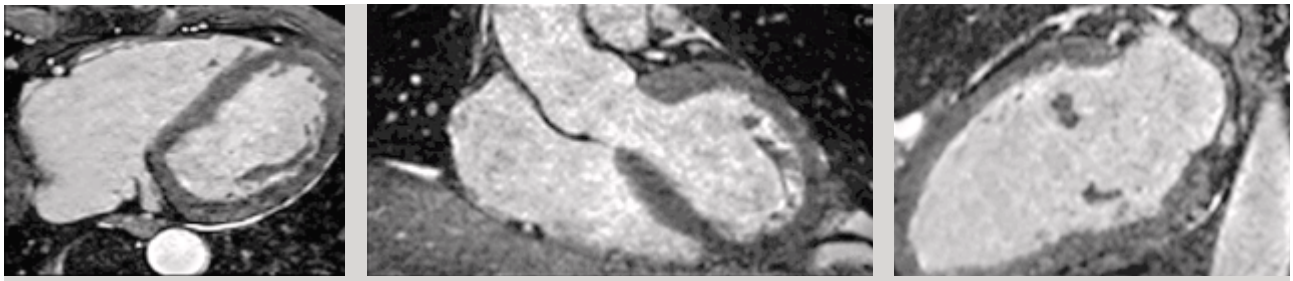

An isotropic 3D TrueFISP data set allows not only the visualization of the complete coronary tree but also a look at cardiac morphology in any orientation, which is especially useful in congenital heart disease. Fast heart rates and small cardiac structures like coronary arteries require highest system performance. The MAGNETOM Avanto system with Tim and iPAT provides excellent results even for the most demanding patients, including children.

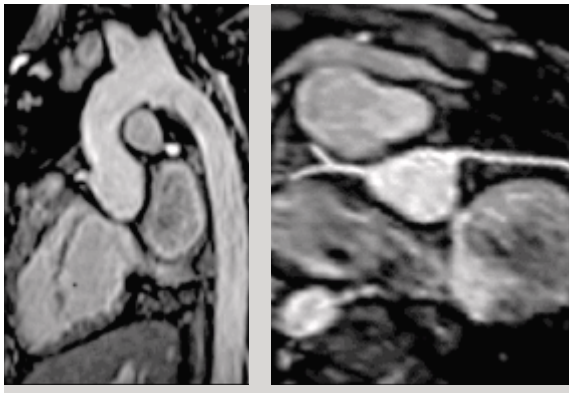

Aortic coarctation after repair, 6-year-old girl, thin MIP images of the aorta and proximal coronaries from an isotropic data set using free-breathing 3D TrueFISP with PACE, acquired in 11:45 min, resolution 1.2 x 1.2 x 1.2 mm^3.

Courtesy of BC Children's Hospital, Vancouver, Canada.

Kawasaki Syndrome, 6-year-old boy, thin MIP images of aneurysms of the coronary vessel shown with free-breathing 3D TrueFISP navigator PACE, acquired in 4:43 min, resolution 1.0 x 1.0 x 1.0 mm^3.

Courtesy of Dr. Abolmaali, Univ. Frankfurt, Germany.

technology (Total imaging matrix) and the MAGNETOM Avanto system, Siemens has now introduced CT-like techniques for coronary imaging in CMR.
The capabilities of Tim and iPAT technology (integrated Parallel Imaging Technique) together with the MAGNETOM Avanto system's hardware performance (fast gradients, excellent homogeneity), Siemens CMR techniques now allow you to image the complete 3D coronary vessel tree in one measurement, with easy imaging techniques, similar to CT but without the use of contrast agent, beta-blockers and without radiation. The whole heart can be imaged at a resolution of approximately 0.7 mm, showing even the distal branches of the vessel tree. And with the PACE (Prospective Acquisition Correction) navigator technique, the patient can breathe comfortably and freely during the measurement.

Near-isotropic Sub-millimeter Resolution Shows Distal Branches

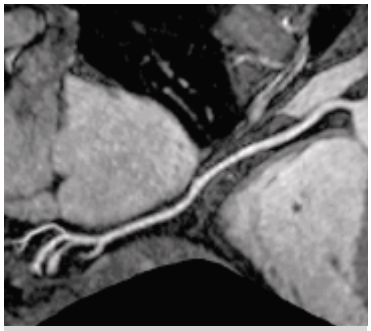

T2-prepared 3D TrueFISP with PACE navigator, acquired in 11 min, resolution 0.7 x 0.7 x 1.1 mm^3, thin MIP images.

Courtesy of Jikei University, Japan.

Marfans syndrome with bypass, 3D TrueFISP with PACE navigator, acquired in 12 min, resolution 1.0 x 1.0 x 1.3 mm^3, thin MIP images.

Courtesy of Dr. Li, Northwestern University, Chicago, USA.

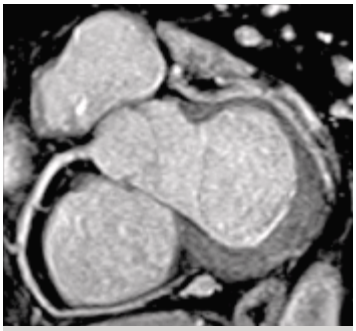

3D TrueFISP with iPAT2, acquired in one breath-hold of 21 s, resolution 1.1 x 1.1 x 1.0 mm^3, thin MIP images.

Courtesy of Drs. Finn, Laub, Deshpande, UCLA, Los Angeles, USA.

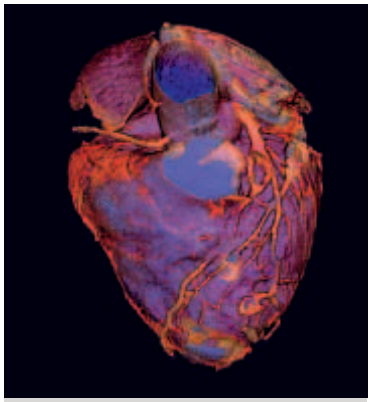

Whole heart coronary MRA acquired with T2-prepared 3D TrueFISP sequence with PACE navigator. Volume rendered images.

Courtesy of Dr. Teraoka, Tokyo Medical University, Tokyo, Japan.

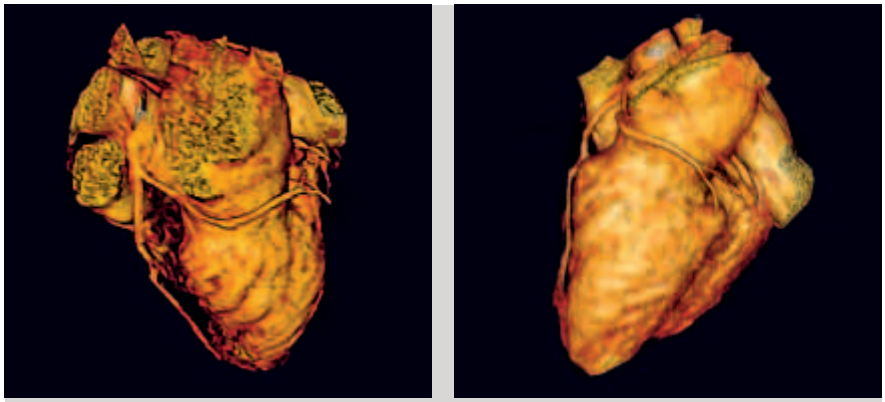

Whole heart coronary MRA acquired with T2-prepared 3D TrueFISP sequence with PACE navigator. Volume rendered images.

Courtesy of Drs. Finn, Laub, Deshpande, UCLA, Los Angeles, USA.

Consistently Excellent Image Quality

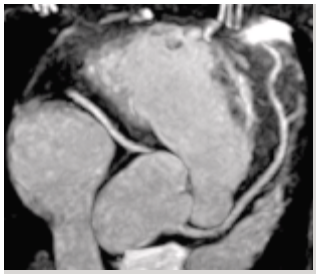

RCA & LAD (Thin MIP)

RCA & LAD (Thin MIP)

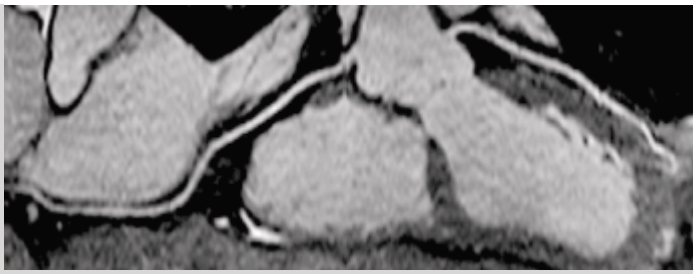

RCA & LAD (Curved Thin MIP)

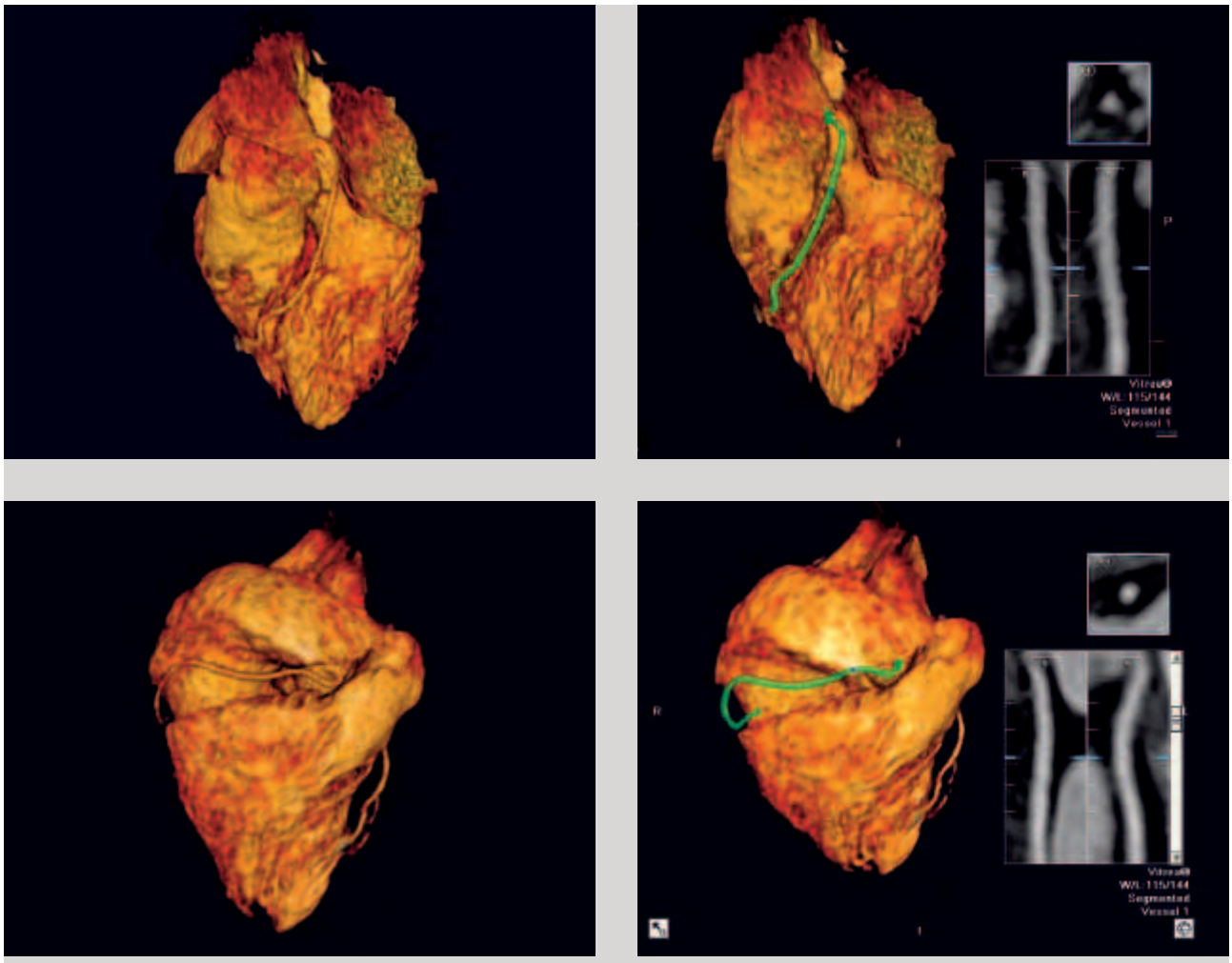

Volume rendered images with automatic vessel tracking (top: LAD, bottom: RCA).

FOV	*190 x 320 mm²*
Matrix	*380 x 640 (i)*
TR/TE	*3.3/1.5 ms*
Flip Angle	*90°*
T2 Prep	*40 ms*

BW	*975 Hz/pixel*
No. of Slices & Slice thickness	*120 Slices @ 1.0 mm (i)*
Time	*10:10 min*
Navigator Acceptance	*69%*

Courtesy of Drs. Finn, Laub, Deshpande, UCLA, Los Angeles, USA

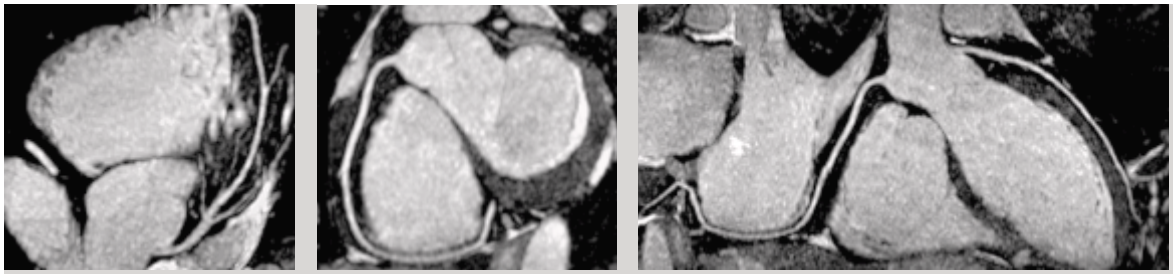

LAD (Thin MIP) *RCA (Thin MIP)* *RCA & LAD (Curved Thin MIP)*

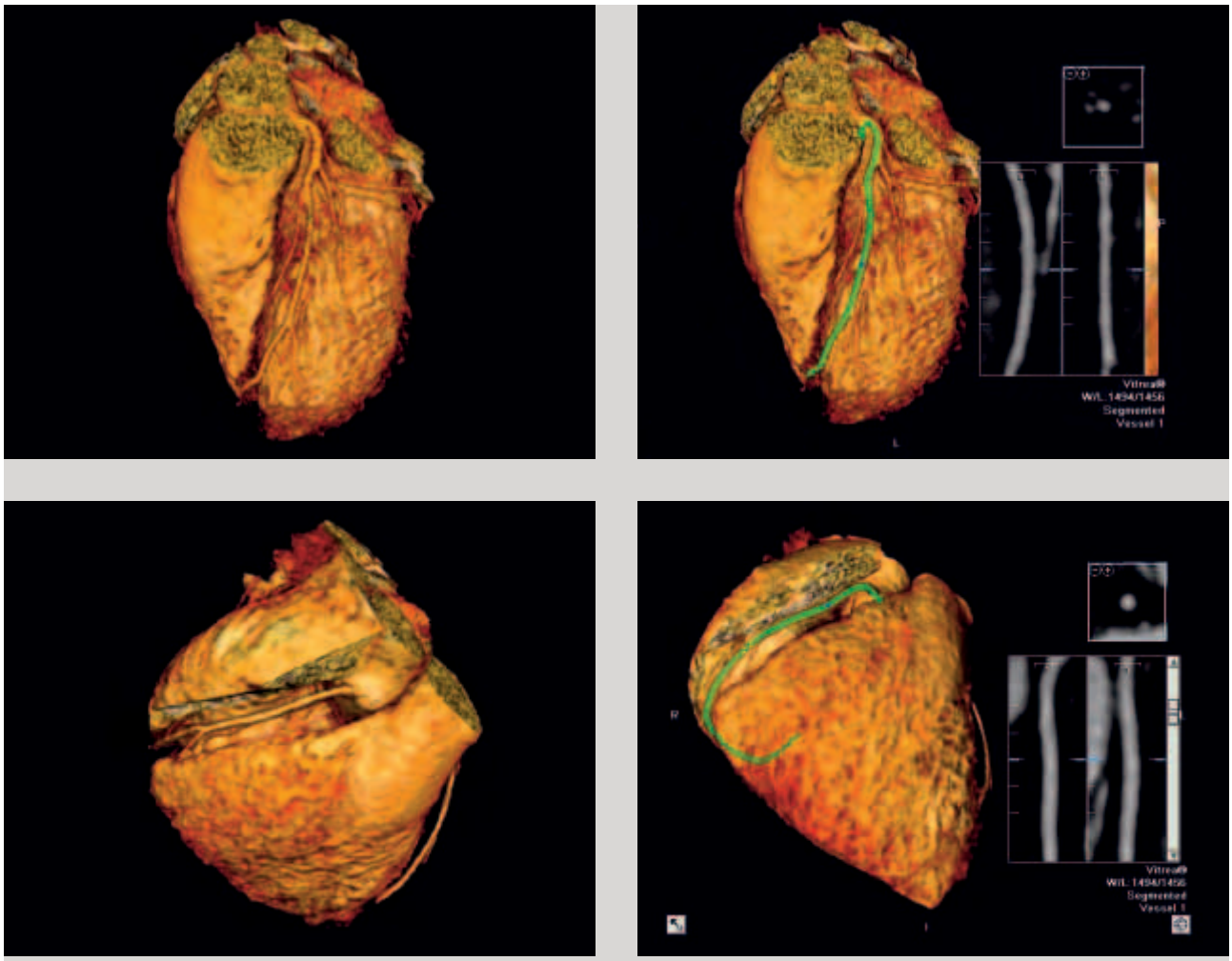

Volume rendered images with automatic vessel tracking (top: LAD, bottom: RCA).

FOV	*190 x 320 mm²*
Matrix	*342 x 640 (i) (p2)*
TR/TE	*3.3/1.5 ms*
Flip Angle	*90°*
T2 Prep	*40 ms*

BW	*975 Hz/pixel*
No. of Slices & Slice thickness	*160 Slices @ 0.75 mm (i)*
Time	*8:51 min*
Navigator Acceptance	*56%*

Courtesy of Drs. Finn, Laub, Deshpande, UCLA, Los Angeles, USA

LAD (Thin MIP)

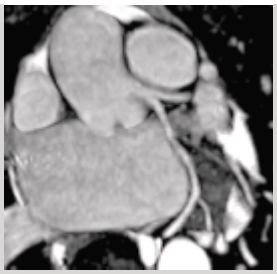

LCX (Thin MIP)

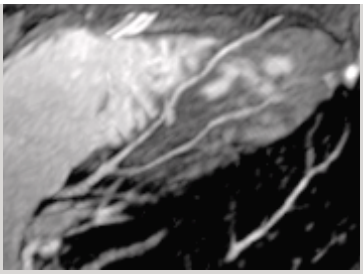

LAD & Diagonal (Thin MIP)

The visualization of major coronary arteries with MRI.

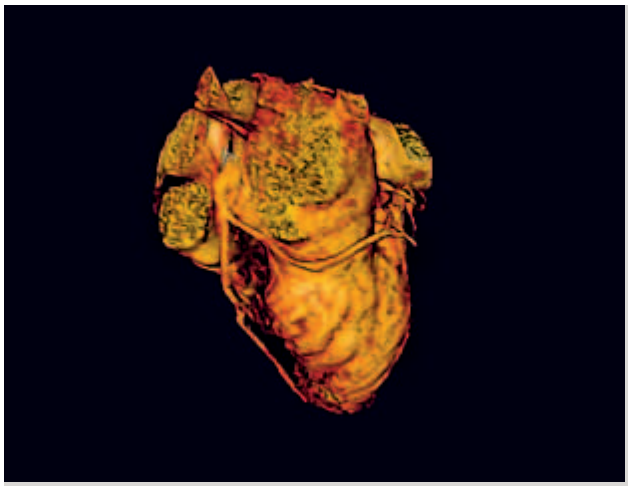

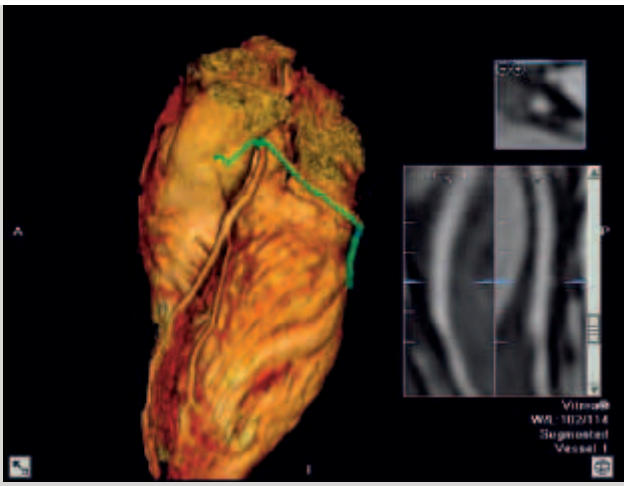

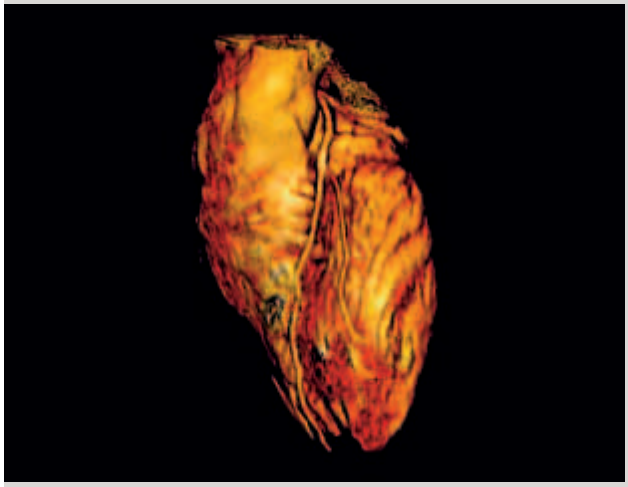

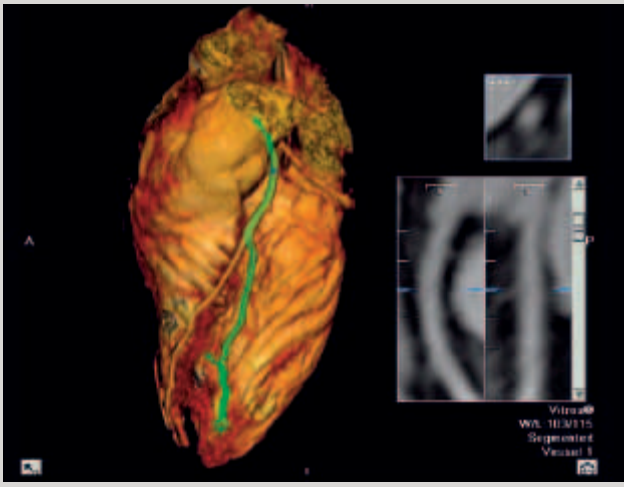

Volume rendered images with automatic vessel tracking (top: LCX, bottom: LAD & Diagonal).

FOV	*190 x 320 mm²*
Matrix	*342 x 640 (i)*
TR/TE	*3.3/1.5 ms*
Flip Angle	*90°*
T2 Prep	*40 ms*

BW	*975 Hz/pixel*
No. of Slices & Slice thickness	*88 Slices @ 1.5 mm (i)*
Time	*11:50 min*
Navigator Acceptance	*42%*

Courtesy of Drs. Finn, Laub, Deshpande, UCLA, Los Angeles, USA

Abbreviations: RCA = Right coronary artery, LAD = Left anterior descending

How does this Fantastic Technology Work?

When using a balanced steady-state free-precession pulse sequence for coronary artery imaging, the data have to be acquired in signal transience to steady-state to preserve the effect of the fat saturation pulse. Therefore, due to the requirement of ECG-triggering, the signal has a relatively strong proton density weighting as opposed to the T2/T1 weighting found in typical steady-state TrueFISP imaging. This reduces the blood-myocardial contrast. As the coronary arteries are in close proximity to fat and myocardial tissue, a higher blood-background contrast is desirable to improve delineation of the vessels. For best contrast in coronary artery imaging, T2-preparation has been added to an ECG-triggered, navigator-gated, fatsat TrueFISP 3D pulse sequence. The basic pulse sequence structure is a segmented 3D approach with 'n' phase-encode lines acquired per heartbeat. The partition gradient is incremented after 'm' heartbeats. In each heartbeat, a T2-preparation is applied after an appropriate trigger delay time, followed by the navigator pulse for respiratory gating, a fat suppression pulse, TrueFISP preparation cycles, data acquisition, and a flipback pulse, followed finally by a gradient spoiler.

This schematic of the ECG-triggered, navigator-gated, T2-prepared, segmented TrueFISP pulse sequence shows the T2prep Pulse (user defined), Navigator Pulses (~40 ms), Fat Suppression Pulse (~20 ms), Linear Flip Angle Preparation Pulses, Data Acquisition Time (user defined), and the Spoiler Pulse (~ 8 ms). The TR shown on the *syngo* user interface taskcard includes all these pulses except the time for the Navigator Pulses. In other words, the time necessary to play out all the sequence events in a cardiac cycle is actually 40 ms greater than the minimum TR in the user interface taskcard. Several new parameters have been added to the Sequence / Specials taskcard: Data Acquisition Time, Trigger to Data Acquisition Time, T2prep Switch, T2prep Time, and Frequency Offset.

Segmented TrueFISP

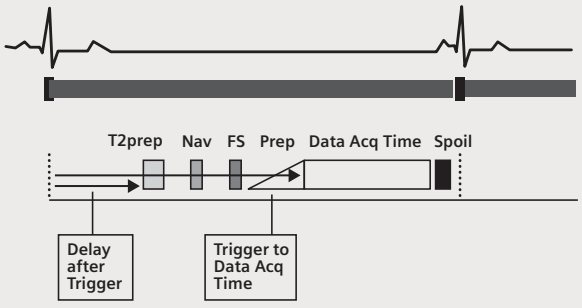

- **Data Acquisition Time:** This parameter defines the duration during which data is acquired.
- **Trigger to Data Acquisition Time:** This parameter will be visible only if triggering is ON. Its value is equal to the time from the R-wave of the ECG trigger to the first line of data acquisition.
- **T2prep Switch:** T2prep can be switched ON or OFF using this switch.
- **T2prep Time:** This parameter will be activated only if the T2prep switch is ON. The T2prep time controls the T2-weighting that the magnetization will undergo before data acquisition.
- **Frequency Offset:** This parameter changes the RF phase cycling in TrueFISP. The phase cycling is equal to 180° when the frequency offset is 0.
- **Frequency Offset**: The frequency offset on the protocol menu changes the phase cycling for the RF pulses. This parameter may be used to optimize the TrueFISP image quality by reducing or eliminating any off-resonance banding artifacts if present. It is recommended that the initial value should be set to 0, and then changed only if necessary. Any change in this parameter does not change the MR frequency used by the system. Therefore, general characteristics, such as fatsat, or slice position do not change when using this frequency offset parameter in the TrueFISP sequence.
- **Navigator Gating:** To acquire a navigator echo, two intersecting slices are excited – one with a 90° pulse and the other with a 180° pulse. The intersection of these slices (a column of tissue) then generates a spin echo, which is used to track the diaphragm (liver-lung boundary). The navigator echo takes approximately 40 ms to run.

How do I Perform the Whole Heart Coronary Exam?

Localizers

1. To estimate the end expiration position of the heart, a free-breathing single slice coronal scout is performed at the level of the heart, with multiple repeated measurements at the same slice position over approximately 18 s. Images that show the end expiration position of the heart will be used to position the imaging slab of the whole heart scan.
2. A free-breathing stack of transverse slices acquired at the dome of the diaphragm will be used to position the navigator pulses of the whole heart scan.

Free-Breathing Cine

1. A free-breathing cine scan is performed to determine the mid-diastolic phase when the heart is relatively stationary. The cine slice is positioned on an axial scout image such that a cross section of the left ventricle is acquired in the cine. The optimal trigger delay and acquisition window for the whole heart scan are determined from the cine images such that data acquisition occurs when the heart is relatively stationary.

2. Find the early to mid diastolic image in the cine series when the heart first stops moving, and note the "TT" time from that image as T_{start}.

3. Find the mid to end diastolic image in the cine series when the heart starts again moving, and note the "TT" time from the prior image as T_{end}.

Whole Heart Protocol Optimization

1. Calculate the optimal data acquisition window as $T_{opt} = T_{end} - T_{start}$ and adjust the number of "Segments" on the Physio Taskcard until the "Data Acquisition Time" on the Sequence / Specials Taskcard is equal to or slightly less than T_{opt}.

2. On the Physio Taskcard set the "TR" to its minimum value, set the "Trigger Delay" to 0, and set the "Acquisition Window" to T_{end}.

3. On the Physio Taskcard adjust "Trigger Delay" such that the "Trigger to Data Acquisition Time" on the Sequence / Specials Taskcard is equal to or slightly greater than T_{start}.

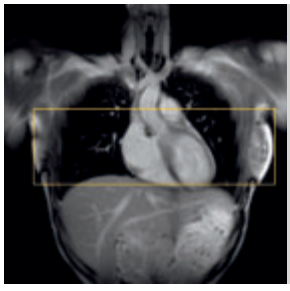

Whole Heart 3D Imaging Slab Positioning
The high-resolution axial 3D imaging slab is positioned on a coronal scout image showing the heart at its end-expiratory position. The number of 3D partitions may be adjusted as needed to cover the heart from base to apex. However, the more partitions used, the longer the scan will be.

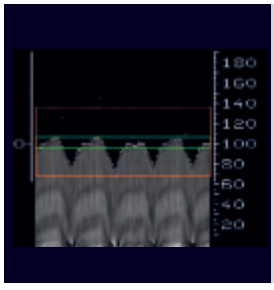

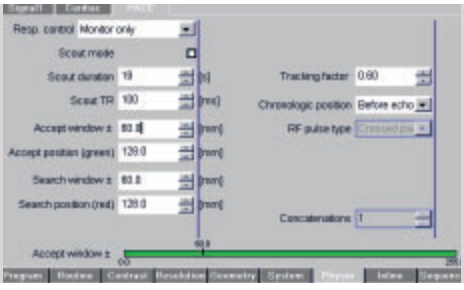

Whole Heart Navigator Scout Mode
The sequence should be run with Scout Mode ON (Physio / PACE Taskcard) to determine if the data acceptance window (green box) coincides with the end-expiratory peaks of the respiratory waveform. If necessary, adjust the Acceptance Position (green), then repeat with Scout Mode ON to ensure correct positioning.

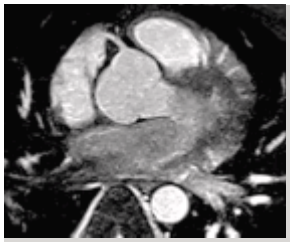

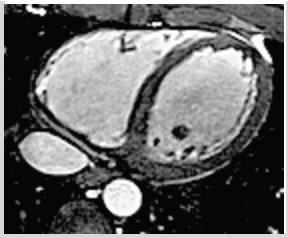

Original Axial Slices

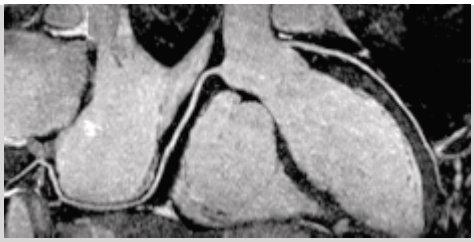

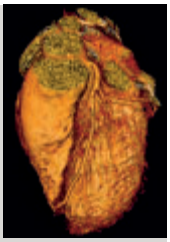

Curved Thin MIP & Volume Rendered

Whole Heart Image Acquisition Mode
Turn the Scout Mode OFF and run the sequence to acquire the image data as a free-breathing exam. The scan time will vary depending upon heart rate, respiration rate, spatial resolution, and acceptance rate (typically 5–10 min). Original axial images should be reviewed as well as Thin-MIP and Volume-Rendered images.

Head and Neck

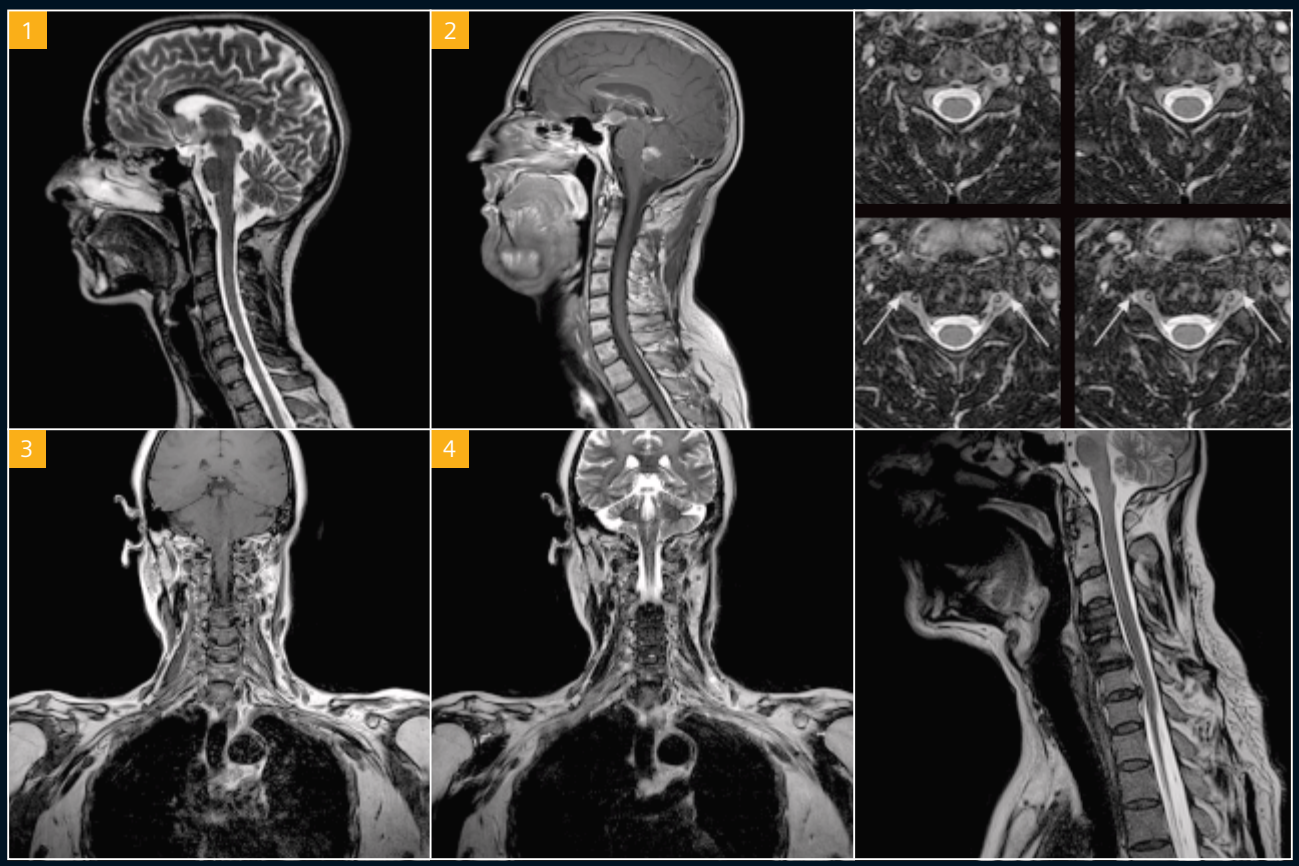

[1, 2] Courtesy of NYU, New York, USA
[3, 4] Courtesy of HKSK, Hong Kong

Non-EPI Diffusion-Weighted MR Imaging in the Diagnosis of Cholesteatoma

Bert De Foer, M.D.[1], Bernard Pilet, M.D.[1], Jean-Phillipe Vercruysse, M.D.[2], Jan W. Casselman, M.D. Ph.D.[1,3]

[1]*Department of Radiology, A.Z. Sint-Augustinus, Antwerp, Belgium*
[2]*University Department of ENT, A.Z. Sint-Augustinus, Antwerp, Belgium*
[3]*Department of Radiology, A.Z. Sint-Jan AV, Bruges, Belgium*

Introduction

MR imaging has an additional value in the detection and delineation of congenital temporal bone and acquired middle ear cholesteatoma. The combination of standard MRI sequences with intravenous gadolinium administration and Spin Echo Echo Planar Diffusion-Weighted (SE EPI DWI) images seems to have – up until now – the highest sensitivity. However SE EPI DWI still has major limitations due to susceptibility-related artefacts, relatively thick slices and low spatial resolution. We report our first experience with a single-shot Turbo Spin Echo diffusion-weighted imaging (single-shot TSE DWI) sequence for the detection and delineation of middle ear cholesteatoma, as well as congenital cholesteatoma, primary acquired cholesteatoma and pre-second look residual cholesteatoma.

MRI Protocol

The protocol for imaging cholesteatoma in our institution consists of 5 sequences. Images are acquired 45 minutes after the intravenous administration of gadolinium on a MAGNETOM Avanto using the standard Head Matrix coil and 2 locally built 7 cm surface ring coils, each connected via its own flex interface. The main difference between SE EPI DWI and single-shot TSE DWI is that the latter sequence uses a 180° RF refocusing pulse for each measured echo.

Protocol for imaging cholesteatoma

Sequence name	Slice orientation	Matrix	SL (mm)	FOV (mm x mm)	Position
TSE T2-WI	coronal	192 x 256	2,0	128 x 170	Suspected pathological ear
Ss TSE DWI	coronal	134 x 192	3,0	220 x 220	Both ears
3D TSE T2-WI	transverse	228 x 448	0,4	107 x 210	Both ears
TSE T1-WI	coronal	192 x 256	2,0	128 x 170	Suspected pathological ear
TSE T1-WI	transverse	144 x 256	2,0	128 x 170	Suspected pathological ear

The total examination time is about 23 minutes.

Case Report 1

13-year-old girl presenting with a small epitympanic congenital cholesteatoma at otoscopy.

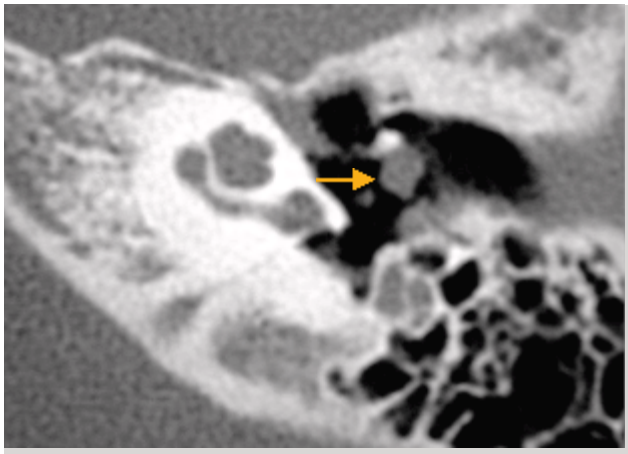

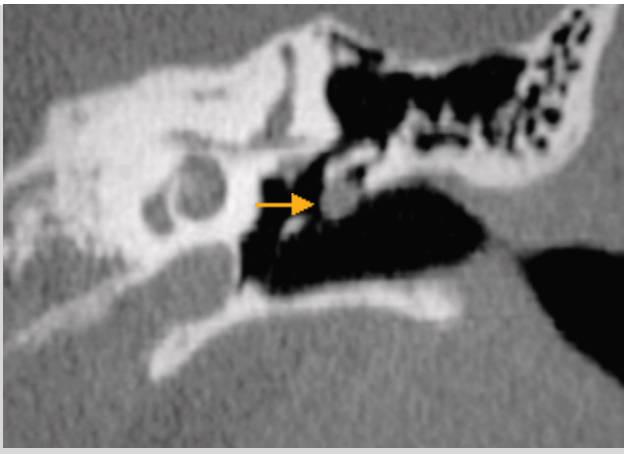

[Figure 1A] *Transverse and coronal high resolution CT image shows a small soft tissue lesion adjacent to the neck of the hammer suggestive of a small cholesteatoma (arrows). The intact tympanic membrane and the lack of chronic inflammatory alterations in the middle ear suggest a small congenital cholesteatoma (size 2 to 3 mm).*

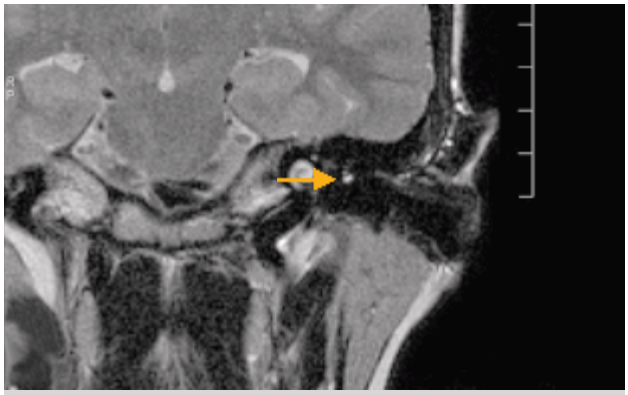

[Figure 1B] *Coronal T2-weighted imaging (T2-WI) shows a small hyperintense nodular lesion in the signal loss region of the temporal bone (arrow). When comparing to Figure 1a the small hyperintense nodular lesions present the small congenital cholesteatoma*

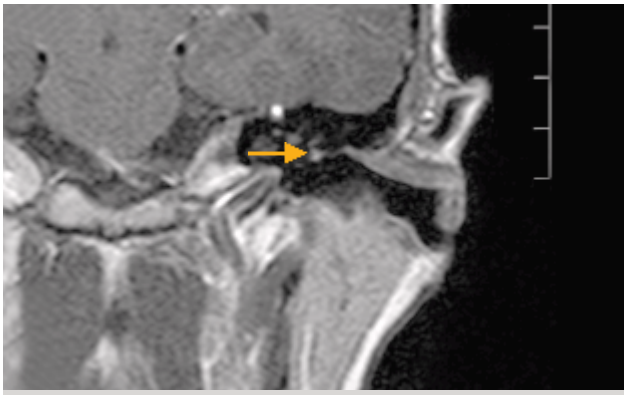

[Figure 1C] *Coronal T1-weighted imaging (T1-WI) shows a small nodular lesion in the temporal bone corresponding to the small congenital cholesteatoma (arrow).*

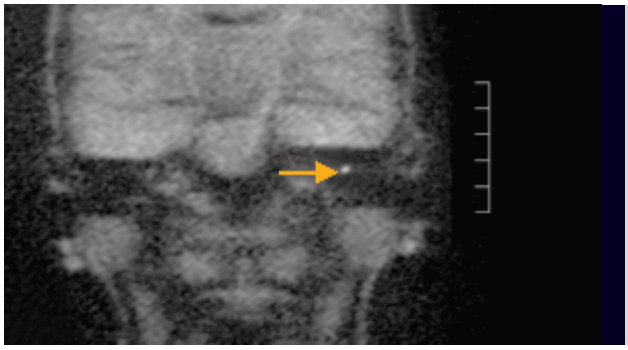

[Figure 1D] *Coronal single-shot Turbo Spin Echo Diffusion-weighted imaging (TSE DWI) clearly shows the small hyperintensity in the temporal bone corresponding to the small congenital cholesteatoma (arrow).*

Case Report 2

76-year-old male with chronic ear discharge.

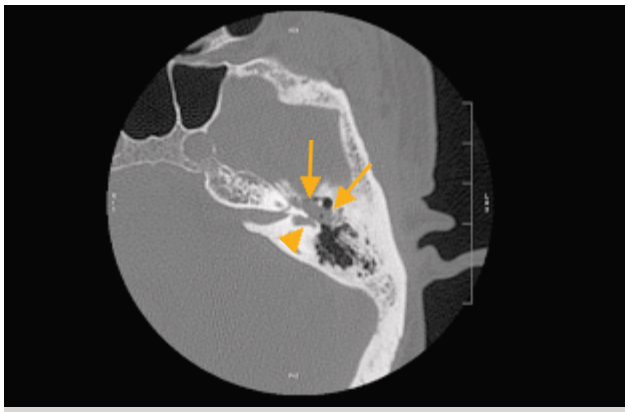

[Figure 2A] *Transverse high resolution CT image shows soft tissue in the attic (arrows) with ossicular erosion and disruption of the anterior part of the lateral semicircular canal (arrowhead).*

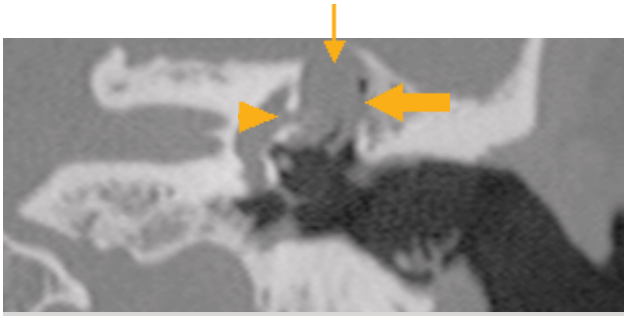

[Figure 2B] *Coronal reformation of a transverse multi slice data set clearly shows the lesion in the attic (large arrow) with suspected erosion of the tegmen (small arrow) and the lateral semicircular canal (arrowhead).*

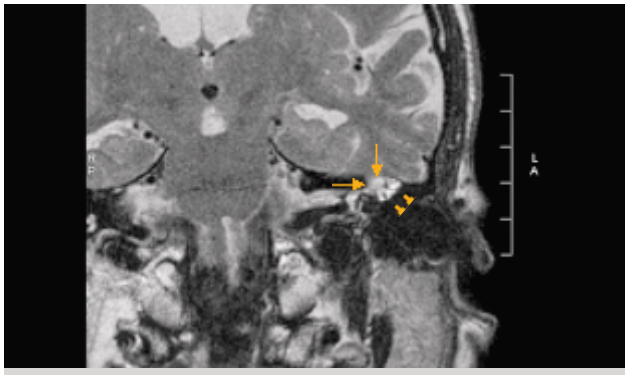

[Figure 2C] *Coronal TSE T2-WI through the temporal bone at the level of the lateral semicircular canal clearly shows the slightly hyperintense cholesteatoma (arrows) surrounded by hyperintense fluid (arrowheads).*

[Figure 2D] *Coronal TSE T1-WI (same level as 2C) 45' after iv Gd shows the enhancing inflammatory tissue (arrowheads) in middle ear and attic surrounding the non-enhancing cholesteatoma under the tegmen (arrows).*

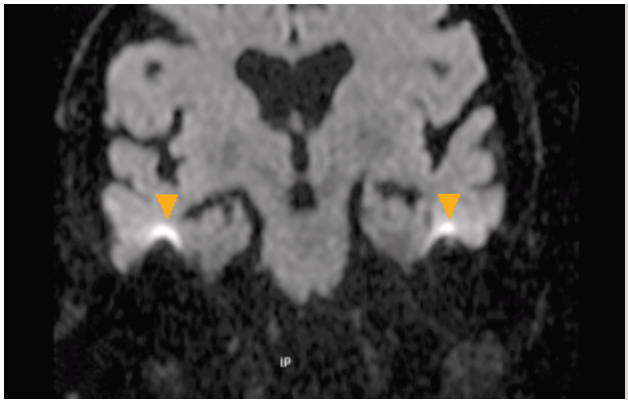

[Figure 2E] *Coronal SE EPI DWI shows the typical interface artefact between temporal lobe and temporal bone (arrowheads). The cholesteatoma cannot be seen due to the artefact.*

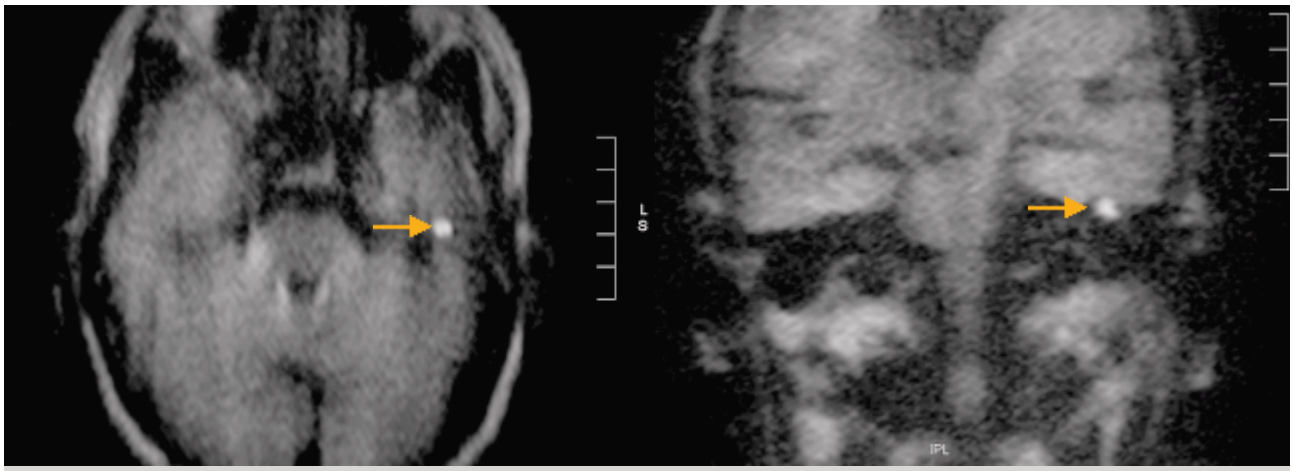

[Figure 2F] *Coronal and transverse single-shot TSE DWI clearly show the small very hyperintense lesion under the tegmen on the left side compatible with cholesteatoma. Note the complete lack of artefacts at the interface between temporal lobe and temporal bone. The lesion can be clearly visualized on both transverse and coronal images (arrows). Compare to figure 2E. In retrospect, the lesion can merely be suspected in the interface artefact of figure 2E on the left side.*

Case Report 3

17-year-old boy with prior surgery for cholesteatoma with primary bony obliteration technique on both sides. In this technique the mastoidectomy cavity is filled with bone chips and bone paté in order to avoid recurrent cholesteatoma. Patient was presented for evaluation of the right side.

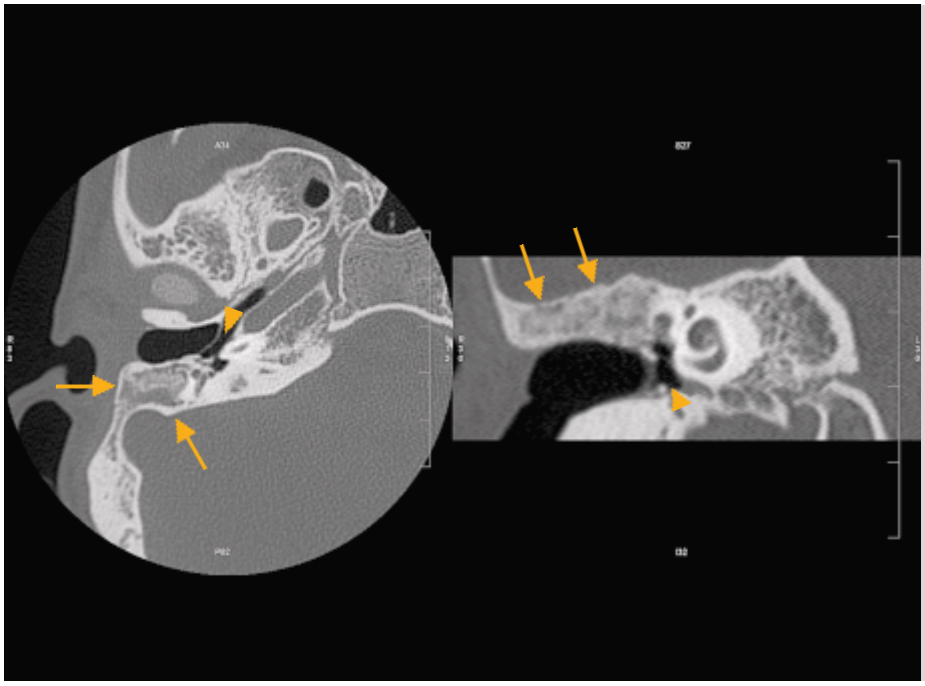

[Figure 3A] *Transverse and coronal CT images show a complete homogeneous opacification of the right mastoidectomy cavity with bony material (arrows). The residual middle ear cavity remains well aerated (arrowheads). On CT, there is no suspicion for cholesteatoma in the obliterated cavity nor in the aerated residual middle ear cavity on the right side.*

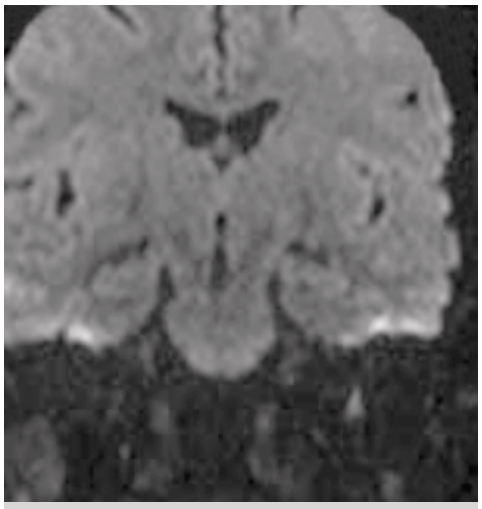

[Figure 3B] *Coronal SE EPI DWI shows no clear hyperintense abnormalities on either right or left side.*

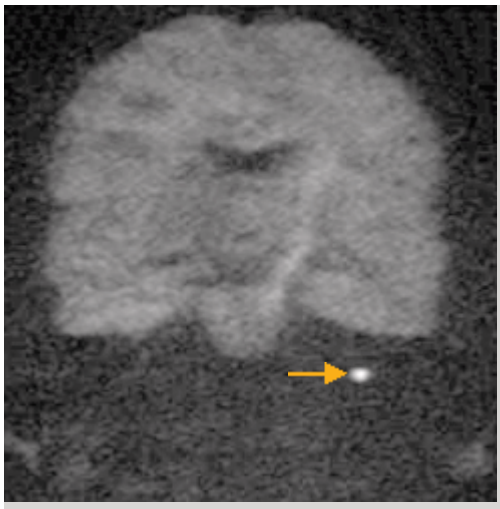

[Figure 3C] *Coronal single-shot TSE DWI shows no clear hyperintensity on the right side but, surprisingly, there is a clear nodular hyperintensity on the left side (arrow), suggestive of a small residual cholesteatoma. Compare to figure 3B. Note the homogeneous signal of the lesion and the complete absence of the interface artefact.*

[Figure 3D] *TSE T1-WI 45' after iv Gd shows a corresponding nodular non-enhancing lesion in the hypotympanon on the left side (arrows), compatible with a small residual cholesteatoma.*

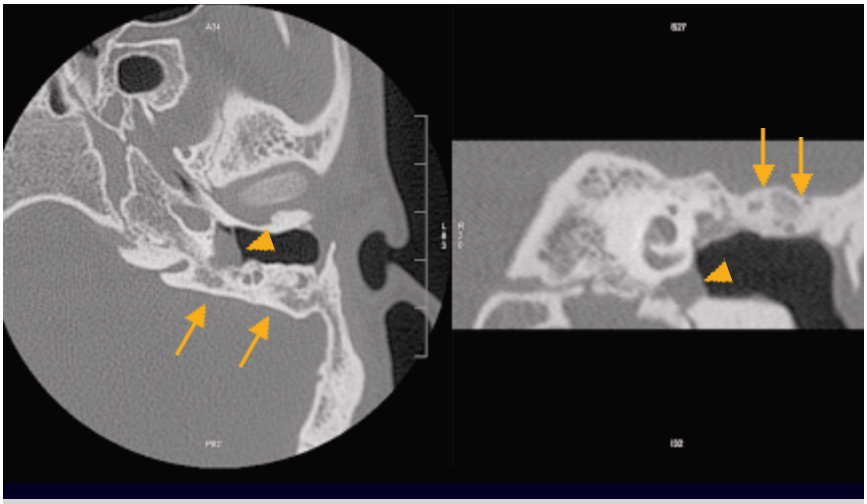

[Figure 3E] *Transverse and coronal CT image through the left middle ear shows a complete and homogeneous opacification of the left mastoidectomy cavity with bony material (arrows). There is a clear nodular soft tissue lesion in the hypotympanum compatible with a cholesteatoma (arrowheads). Compare to figure 3C and 3D.*

Discussion

High resolution CT scan still remains the primary examination tool for the evaluation of a patient suspected of having a middle ear cholesteatoma. It gives excellent information on the extension of the lesion, ossicular erosion and delineation of the tympanic segment of the facial nerve. It also clearly reveals erosion of the lateral semicircular canal and tegmen (1). In selected cases, MRI has an additional value for the evaluation of cholesteatoma extension and for the assessment of

possible complications such as erosion of the lateral semicircular canal, invasion in the membranous labyrinth and invasion in the middle cranial fossa through an eroded tegmen (1). Several past reports have discussed the aspect of cholesteatoma on MRI. The aspect of a congenital temporal bone cholesteatoma or an acquired cholesteatoma on standard MRI sequences is well known. On T2-weighted images cholesteatoma has a slightly higher signal intensity than brain tissue (gray matter). On T1-weighted images, it has an isointense appearance with peripheral matrix enhancement. As cholesteatoma is avascular tissue, the center of the cholesteatoma never enhances contrary to inflammatory and/or granulation tissue (2, 3).

Recently, the aspect of cholesteatomatous tissue on echo planar diffusion-weighted MR images (SE EPI DWI) has been described. Congenital temporal bone cholesteatoma as well as acquired middle ear cholesteatoma exhibit a high signal on SE EPI DWI probably caused by a combination of restricted diffusion and a T2-shine through effect (4, 5, 6, 7). The major limitation seems to be the important air-bone interface artefact at the skull base, the distortion of the images and the low spatial resolution. Furthermore, smaller lesions (less than 5 mm) are still missed using the SE EPI DWI (8).

Moreover, in the past, several studies have shown the failure of MRI in demonstrating and delineating residual cholesteatoma before second-look surgery (9, 10). Therefore, second-look surgery, performed about one year after first-look surgery, remains the gold standard for detection of residual cholesteatoma up until now.

The combination of standard post-contrast MRI sequences combined with SE EPI DWI -up until now- seems to have the highest sensitivity for the detection of residual cholesteatoma. Again, a high number of residual cholesteatomas can be missed due to the often small size of these residual cholesteatoma pearls (2 to 4 mm) and the air-bone interface artefact noted at the skull base (8, 11, 12, 13, 14).

Recently, the use of late post-contrast T1-weighted images has been demonstrated to be of a great value in differentiating cholesteatoma from inflammatory and granulation tissue. It is stated that post-operative inflammatory and granulation tissue show a slow centripetal contrast uptake and can thus only be differentiated from (non-enhancing) cholesteatomatous tissue by using late post-contrast T1-WI images (15, 16).

By using single-shot TSE DWI we succeeded in overruling the above-mentioned major limitations of SE EPI DWI. Our first results show that prior size limitations to cholesteatoma detection seem to be overruled (Fig. 1). Furthermore, single-shot TSE DWI has no interface artefact at the temporal bone – temporal lobe border (Fig. 2). Further investigations and studies using the new combination of late post-contrast T1-WI and single-shot TSE DWI for the detection and delineation of small acquired middle ear cholesteatoma and pre-second look residual cholesteatoma have currently been started. We hope that the combination of late post-contrast T1-WI and single-shot TSE DWI has the highest sensitivity and specificity in order to replace second-look surgery for acquired middle ear cholesteatoma (Fig. 3).

*This information about this product is preliminary. The product is under development and not commercially available in the US and its future availability cannot be ensured

References

[1] Lemmerling M, De Foer B. Imaging of cholesteatomatous and non-cholesteatomatous middle ear disease. In: M. Lemmerling, S.S.Kollias. Radiology of the Petrous Bone, 1st edn. Springer Verlag Berlin Heidelberg New York pp 31–47.

[2] Martin N, Sterkers O, Nahum H. Chronic inflammatory disease of the middle ear cavities: Gd-DTPA-enhanced MR imaging. Radiology. 1990; 176: 399–405.

[3] Ishii K, Takahashi S, Kobayashi T, et al. MR imaging of middle ear cholesteatomas. J Comput Assit Tomogr. 1991; 15: 934–937.

[4] Robert Y, Carcasset S, Rocourt N, et al. Congenital cholesteatoma of the temporal bone: MR findings and comparison with CT. Am J Neuroradiol 1995; 16: 755–761.

[5] Fitzek C, Mewes T, Fitzek S, et al. Diffusion-weighted MRI of cholesteatomas of the petrous bone. J Magn Reson Imaging 2002; 15: 636–641.

[6] Maheshwari S, Mukherji SK. Diffusion-weighted imaging for differentiating recurrent cholesteatoma from granulation tissue after mastoidectomy: case report. Am J Neuroradiol 2002; 23: 847–849.

[7] Mark AS, Casselman JW. Anatomy and disease of the temporal bone. In: Atlas SW, Eds. Magnetic Resonance imaging of the brain and spine, 3rd edn. Philadelphia: Lippincott, Williams and Wilkins, 2001; 1363–1432.

[8] De Foer B, Casselman JW, Govaere F, et al. The role of MRI and diffusion-weighted images in the diagnosis of middle ear cholesteatoma. Acta Radiol Port 2002; 14: 89 (abstract).

[9] Kimitsuki T, Suda Y, Kawano H, et al. Correlation between MRI findings and second-look operation in cholesteatoma surgery. ORL J Otorhinolaryngol Relat Spec. 2001; 63: 291–3.

[10] Vanden Abeele D, Coen E, Parizel PM, et al. Can MRI replace a second look operation in cholesteatoma surgery? Acta Otolaryngol. 1999; 119: 555–61.

[11] Aikele P, Kittner T, Offergeld C, et al. Diffusion-weighted MR imaging of cholesteatoma in pediatric and adult patients who have undergone middle ear surgery. AJR Am J Roentgenol. 2003 ; 181: 261–5.

[12] Stasolla A, Magluilo G, Parrott D, et al. Detection of Postoperative Relapsing/Residual Cholesteatomas with diffusion-weighted echo-planar magnetic resonance imaging. Otol Neurotol 2004: 25; 879–884.

[13] J-Ph Vercruysse, B. De Foer et al. The value of Diffusion-Weighted MR-imaging in the Diagnosis of Primary Acquired and Residual Cholesteatoma: a surgical verified study in 100 patients. Submitted for European Radiology.

[14] B. De Foer, J-Ph Vercruysse et al. The value of high resolution CT and MR imaging including diffusion-weighted images in the detection of post-operative residuel cholesteatoma. Submitted for European Radiology.

[15] Williams MT, Ayache D, Alberti C, et al. Detection of postoperative residual cholesteatoma with delayed contrast-enhanced MR imaging initial findings. Eur Radiol. 2003; 13: 169–74.

[16] Veillon F, Riehm S, Enachescu B, et al. Diffusion versus delayed post gadolinium FAT-SAT T1-weighted imaging of cholesteatoma of the petrous bone. Acta Radiol Port 2002; 14: 89 (abstract).

The Utility of Surface Coils and New Sequences in Orbital and Ocular MR Imaging

Smita Kori, M.D., Meher Ursekar, M.D., Bhavin Jankharia, M.D., Pradeep Krishnan, M.D.

Jankharia Imaging Centre, Mumbai, India

Introduction

MRI of the orbit has become an important diagnostic tool in ophthalmology. The development and refinement of surface coils, increased speed of scanning and newer pulse sequences such as post-contrast dark fluid or FLAIR sequences have improved visualization of fine details of orbital and ocular structures.

We routinely perform high resolution MRI of the orbit when clinically indicated, using phased array coils. Fat suppressed (FS) T1-weighted (T1W), T2-weighted (T2W) and dark fluid sequences are obtained in the axial, coronal and sagittal views. This has helped us in making definitive diagnoses in a number of patients.

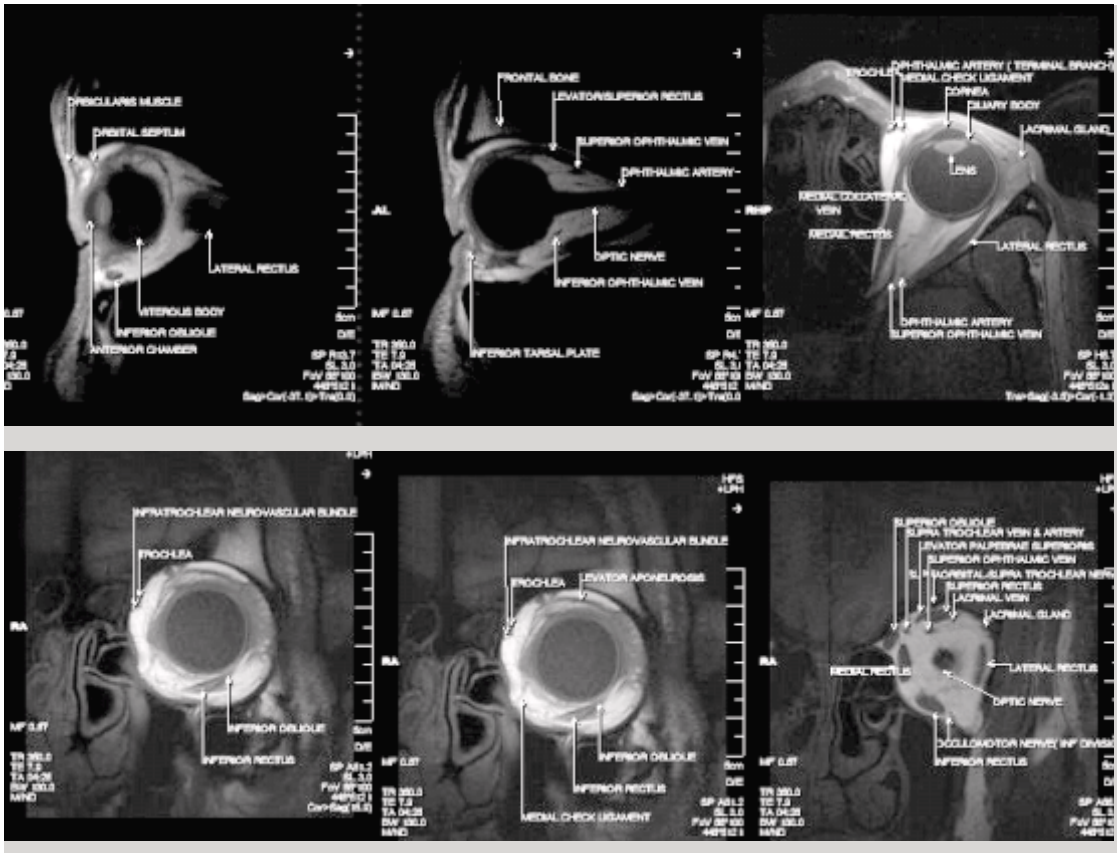

Head coil (T2-weighted)

T2 dark fluid

Comparison of the orbit. *Surface coil and head coil. Ocular layers are clearly seen on the surface coil image. The septum orbitale (arrow) is also well delineated.*

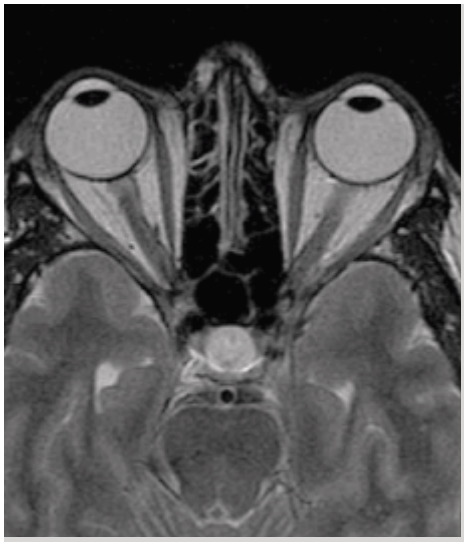

Head coil (T2-weighted)

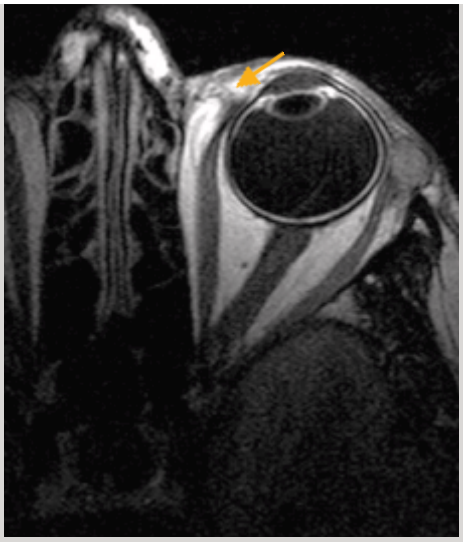

T2 dark fluid

Comparison of the orbit surface coil and head coil. *Ocular layers are clearly seen on the surface coil image. The septum orbitale (arrow) is also well delineated.*

Technique

The patients were instructed to avoid eye movements during the study. Studies were performed on a 1.5 Tesla system (MAGNETOM Sonata, Siemens Medical Solutions, Erlangen) using a surface coil with a 6 cm diameter. Oblique axial and sagittal images were planned parallel to the long axis of the optic nerve.

Findings

The higher spatial resolution coupled with increase in signal-to-noise ratio (SNR) afforded by the use of surface coils combined with rapid scanning (thus reducing motion artifacts), and pulse sequences like dark fluid, allows visualization of small details. Vitreous is effectively suppressed on dark fluid sequences and the ocular layers are better delineated. Small structures like the palpebral layers, septum orbitale and levator aponeurosis are distinguishable, allowing differentiation of the preseptal and postseptal spaces, which is important in orbital disease.

Protocol details

Sequence	TR ms	TE ms	TI	FOV mm	Matrix	S.T	No. slices	Flip angle	Band width	Time (min)
T1	350	7.9		100	256 x 256	3	14	90	130	4.32
T2	3000	98		100	512 x 512	3	14	150	130	4.26
Dark fluid	6000	99	2000	100	256 x 179	3	14	150	210	4.38

Case Studies

Complicated Sinusitis: Subperiosteal orbital inflammation secondary to left ethmoid and maxillary sinusitis.

This patient came with a history of pain in the left eye that began 15 days previously.

Post-contrast T1W axial

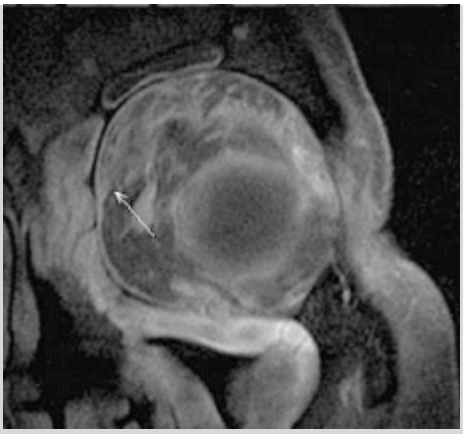

Post-contrast T1W coronal

Findings: *Streaky, enhancing inflammatory soft tissue consistent with orbital cellulitis, displacing the medial rectus and the superior oblique muscles. The good resolution images helped us to confidently exclude loculated abscess, which may have required surgical drainage, and also showed the inflammation to be confined within the postseptal space.*

Myositis of extraocular muscle

An 8-year-old female child presented with pain in the left eye that began 3 weeks previously and mild proptosis.

T1W axial

Post-contrast T1W axial

Findings: *Marked fusiform thickening of the medial rectus muscle of the left orbit, involving the muscle belly with focal indentation of the optic nerve. Heterogeneous enhancement with multiple small foci of necrosis are seen. The anterior tendon insertion was thickened and there was no focal scleral enhancement. There was no infiltration of the septum orbitale, helping to differentiate this from aggressive tumor.*

Optic nerve glioma in Neurofibromatosis type I

T1W axial

T2W axial

Post-contrast T1W fat suppressed coronal

Enlargement of optic nerve is noted. The optic nerve is isointense on the T1W images with hyperintense tumor surrounding the nerve sheath. Septations were seen within it and the rim found to enhance. Infiltration of the intra-canalicular segment of the nerve was seen. The tumor preserves the nerve shape and has a bulky extra-neural component that has infiltrated the sheath. This was well seen on the surface coil study.

Retinal detachment

Dark fluid axial

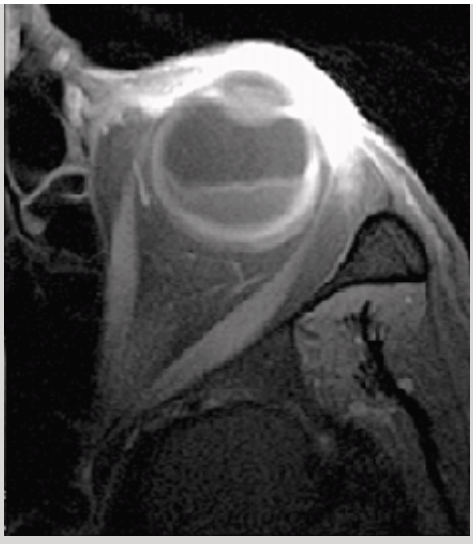

T1W axial

Homogeneous clear fluid is seen to have accumulated beneath the retinal detachment. An underlying focal mass lesion is confidently excluded, but there is diffuse thickening of the choroidal membrane due to hemangioma.

Melanoma

A 47-year-old male presented with reduced vision in the left eye which began 1 week previously.

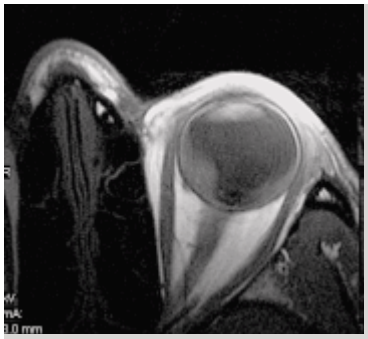

T1W axial

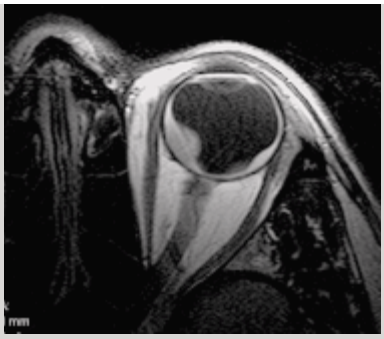

Dark fluid post-contrast axial

A focal nodular enhancing, lesion is seen in the nasal quadrant within the posterior segment of the eye. The lesion is subretinal and is associated with retinal detachment and subretinal effusion. This turned out to be a metastasis.

Lacrimal cyst

A 34-year-old male reported with swelling in the right lateral canthus.

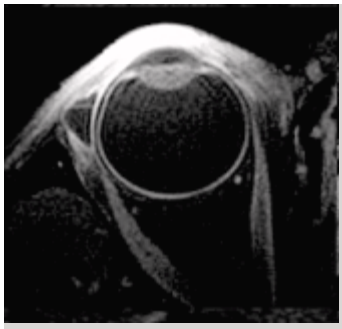

Post-contrast T1W

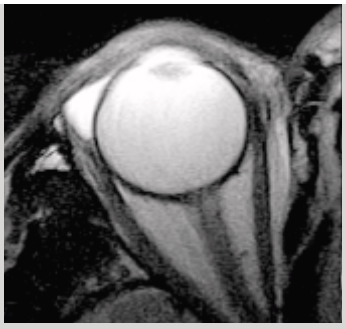

T2W

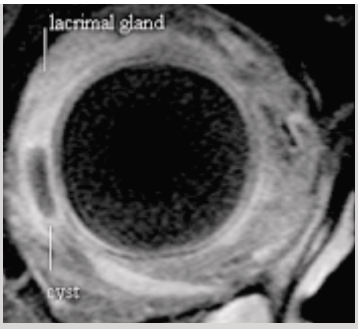

Post-contrast T1W coronal

A cystic lesion is seen in the inferior tip of the lacrimal gland (coronal image) with clear fluid within. The wall is thin and enhances. The insertion of the lateral rectus is uninvolved. Surface coil images helped confirm that the lesion was entirely within the lacrimal and was therefore, probably a benign lacrimal cyst.

Trochlear injury

Patient with head injury 4 months ago. Suspected left trochlear nerve injury.

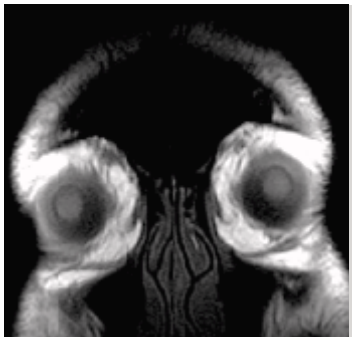

Asymmetry in the thicknesses of the superior oblique muscles is seen, with thinning of the left superior oblique belly anteriorly, near the reflected segment through the trochlea. The thinning of the insertion of the superior oblique muscle was very well appreciated.

Retinal angioma

A 25-year-old female with clinical suspicion of Von Hipple Lindau syndrome reported with complaints of reduced vision in the right eye.

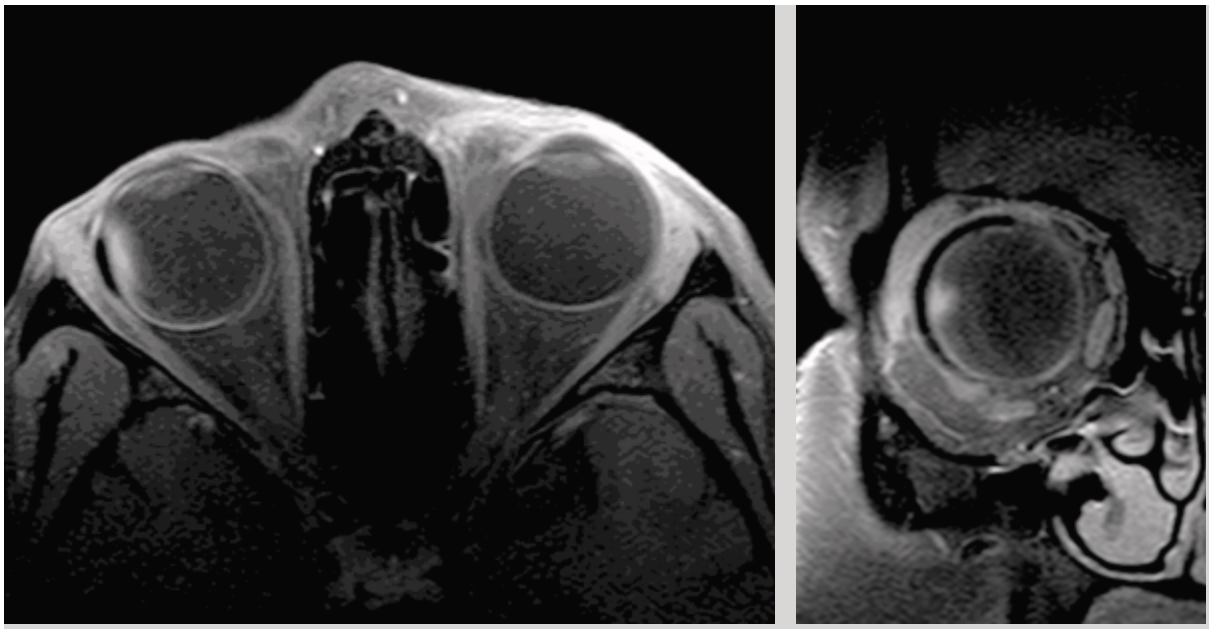

Focal enhancement along the uveal coat in the right globe laterally represents retinal angioma. MRI of the brain showed a small enhancing hemangioblastoma in the inferior vermis.

Extraocular cysticercosis

A 35-year-old male complained of pain in the right eye with accompanying right sided headaches.

T2W Axial

Post-contrast T1W axial

Post-contrast dark fluid axial

A cystic lesion is seen within the belly of the right lateral rectus muscle. The cyst wall is thick and appears relatively hypointense on the T2-weighted images. There is thick enhancement of the cyst wall and surrounding muscle on the post-contrast image. An enhancing internal structure is seen within the cyst only on the high resolution post-contrast, fat suppressed dark fluid or FLAIR sequence. This is diagnostic of the scolex of cysticercus.

Differentiating Primary Parotid Gland Lesions by Diffusion-Weighted MR Imaging

C. R. Habermann[1], M.D., J. Graessner[2], M.Sc., M. C. Cramer[1], M.D., F. Weiss[1], M.D.

[1]*Department of Diagnostic and Interventional Radiology, University of Hamburg, Germany*
[2]*Siemens AG, Medical Solutions, Hamburg, Germany*

Introduction

The most important clinical application of Diffusion-weighted (DW) magnetic resonance imaging (MRI) is the detection and characterization of cerebral ischemia (1). Recently, a few studies were published to determine the value of DW MRI in healthy parotid glands and systemic disorders affecting parotid glands by measuring ADC values under physiologic and pathologic conditions, or after irradiation (2–4).

In the Department of Otorhinolaryngology in Hamburg, Germany between 80 and 120 patients with tumors are operatively treated per year. Comparable to the literature, between 60 to 80% of these patients suffer from pleomorphic adenoma or Warthin tumors. The missing twenty percent show primary malignant tumors of the parotid gland, or prove to have metastatic disease within the parotid gland. So, most patients are treated under the assumption of a benign primary disease. The difficulty is not only that the operative approach differs among benign and malignant tumorous disease but also that pleomorphic adenoma has to be treated more aggressively in comparison to Warthin tumors, due to their higher recurrence rate (5).

Methods

All examinations were performed using a MAGNETOM Symphony with a Quantum gradient system, with 30 mT/m maximum gradient capability and a maximum slew rate of 125 mT/m/sec. The lower part of the circularly polarized (CP) head coil and a standard two-element CP neck array coil were used. The flexibility of the neck array coil allowed positioning the N1 element right next to the parotid gland. An axial diffusion-weighted EPI (echo-planar imaging) sequence (TR 1,500 ms / TE 77 ms) was obtained with a matrix of 119 x 128, a field of view of 250 x 250 mm (pixel size 2.10 x 1.95 mm), 6 excitations, and a section thickness of 5 mm with an interslice gap of 1 mm. A parallel imaging technique (modified Sensitivity Encoding algorithm (mSENSE)) with an acceleration factor of two with twelve additional lines for self calibrating was applied. A bandwidth of 1502 Hz/pixel was used and 12 slices were acquired. The b factors used were 0 s/mm^2, 500 s/mm^2 and 1,000 s/mm^2. Fat suppression was achieved by placing the frequency-selective radio-frequency pulse before the pulse sequence. The automatic 3D-shim routine of the magnet used the slice block as the shim volume. The total acquisition time of this sequence was 1:14 mins.

Evaluation of the ADC maps were performed using the analyzing software MRIcro (Chris Rorden, University of Nottingham, Great Britain), which lists every pixel intensity of each ADC slice in a single ROI output file per patient.

Conclusion

DW MR imaging seems to be a valuable tool to differentiate not only benign from malignant lesions, as shown in the two patients above, but also to differentiate between malignant and benign primary lesions of parotid glands (6). In our ENT department it has become an obligatory second line imaging tool prior to surgery for planning the operative strategy. Up to now, 135 patients with primary lesions of parotid and submandibular glands were examined with DW MR imaging, with no failure to provide the diagnosis.

References

[1] Fiehler J, Fiebach JB, Gass A, et al. Diffusion-weighted imaging in acute stroke – a tool of uncertain value? Cerebrovasc Dis 2002; 14: 187–196.

[2] Sumi M, Takagi Y, Uetani M, et al. Diffusion-weighted echoplanar MR imaging of the salivary glands. AJR Am J Roentgenol 2002; 178: 959–965.

[3] Patel RR, Carlos RC, Midia M, Mukherji SK. Apparent diffusion coefficient mapping of the normal parotid gland and parotid involvement in patients with systemic connective tissue disorders. AJNR Am J Neuroradiol 2004; 25: 16–20.

[4] Habermann CR, Cramer MC, Graessner J, et al. Functional imaging of parotid glands: diffusion-weighted echo-planar MRI before and after stimulation. Rofo 2004; 176: 1385–1389.

[5] Donovan DT, Conley JJ. Capsular significance in parotid tumor surgery: reality and myths of lateral lobectomy. Laryngoscope 1984; 94: 324–329.

[6] Habermann CR, Gossrau P, Graessner J, et al. Diffusion-weighted echo-planar MRI: a valuable tool for differentiating primary parotid gland tumors? Rofo 2005; 177: 940–945.

Case 1

46-year-old female patient with a palpable, painless mass of the right cheek.

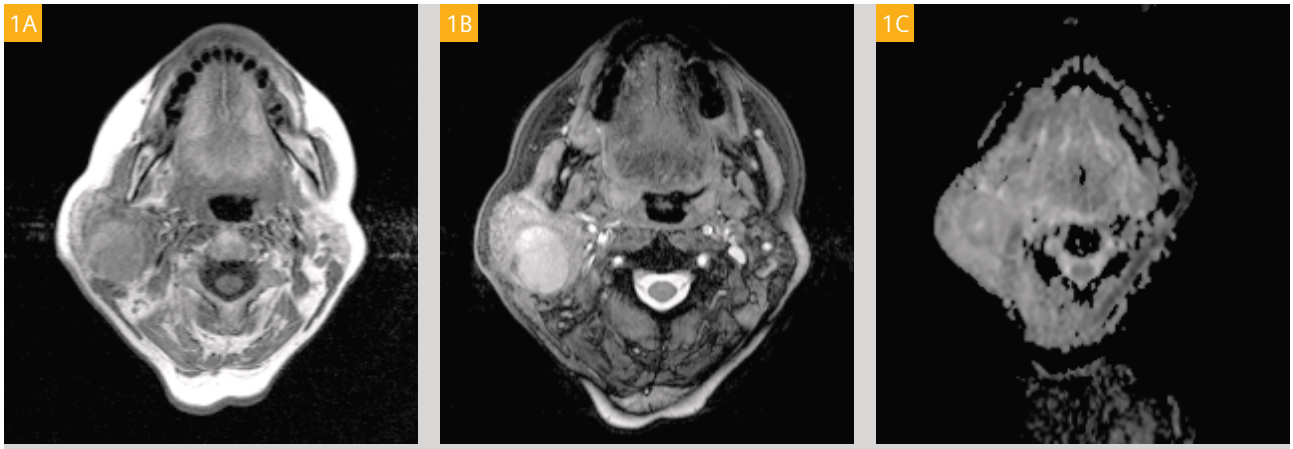

The T1-weighted images (1) showed a tumor in the right parotid gland with muscle isointense appearance. The T2-weighted images (A) showed an intraparotideal mass with higher signal intensity as the surrounding parotid gland tissue and the muscles. Concerning the ADC images a fairly low value could be obtained (1.28 x 10–3 $mm^2/s \pm 0.11 \times 10–3\ mm^2/s$). Images show a histologically proven salivary duct carcinoma.

Case 2

76-year-old male patient with a palpable, painless mass of the right cheek.

The morphologic appearance of this tumor is very similar to the tumor presented in case 1. In both patients contrast enhancement gave no additional information regarding the tumor. In contrast to case 1, the ADC images showed an obvious higher diffusion within the tumor (2.06 x 10–3 $mm^2/s \pm 0.15 \times 10–3\ mm^2/s$). Histology revealed a pleomorphic adenoma.

3T Ultra High-Field Intraoperative MR with Twin Room Concept

Alp Dinçer, M.D.[1], M.Necmettin Pamir, M.D.[2]

Acibadem Kozyatağı Hospital, Dept. of Radiology (1) and Neurosurgery (2), Istanbul, Turkey

Introduction

Intraoperative MR (IoMR) has gained acceptance over the last decades. IoMR during neurosurgical intervention has allowed not only improvement of the precision of navigation, optimization of the surgical approach and maximal preservation of normal brain tissue and function, but also an assessment of the completeness of tumor resection and the ability to exclude surgical complication (1). As IoMR has been evolving, many different system configurations – with their own advantages and disadvantages – have been developed (1–3). The main disadvantage of low field scanners is low SNR that affects not only the image quality and scan time, but also restricts the many new intraoperative applications such as functional MR, MR Spectroscopy (MRS), and Diffusion Tensor Imaging (DTI) Fiber Tractography. As the image quality is strictly related to the strength and homogeneity of the static and gradient magnetic fields, we chose the state-of-the-art 3T MR system for our dedicated neurosurgery hospital to be able to perform newer MR applications. Due to economic trade-offs (with our approach), instead of putting the magnet in the operating room, we preferred the twin room concept with a floating table that allows the transfer of the patient from one room to another easily. Furthermore, this configuration allows us to use every kind of surgical equipment including the microscope out of the 5 Gauss line without any compromise.

Method

Our 3T MRI site is built next to the operating theatre dedicated to neurosurgical operations. The magnet room and the operating theatre, which are connected to each other by a door, are both RF-shielded. In daily practice, we use the 3T MRI (MAGNETOM Trio, Siemens, Erlangen) as a clinical scanner. Before the operation, the magnet and the console rooms are disinfected. Whenever the neurosurgeon needs imaging during the operation, the door between the magnet room and the operating theatre is opened, and the patient is transferred from the operating table to the magnet cradle with a floating table in a maximum of three minutes. All of the equipment in the magnet room is compatible with 3T MR. Since all of the surgical equipment including the microscope is out of the 5 Gauss line, we can use all of it safely. Initially, we used the body coil to transmit and receive signal in 25 patients because we did not have the head coil compatible with the head holder. Over the last three months, we have used a dedicated head holder with a specially designed 8-channel head coil. Axial, sagittal and/or coronal TSE T2, SE T1 and 3D FLASH T1-weighted images (slice thickness 1–6 mm, gap 0–1 mm, matrix 192-256 x 256-512, FOV 200–260 mm) are obtained according to the lesion. Total examination time including the transfer of the patient, the analysis of the images and the final decision is approximately 10 minutes. At the end of the examination we decide to continue or terminate the operation. If we decide to go on, the examination procedure is repeated. If the operation is terminated, the door between the magnet room and the operating theatre is closed, and routine outpatient examinations begin immediately.

Discussion

The image quality of the MR was acceptable and diagnostic in the examinations using the body coil at the beginning. The image quality and the spatial resolution of the MR exams using the 8-channel head coil are excellent without any compromise. Hemorrhage and susceptibility do not cause any significant artifacts at the high 3T field strength. There were no complications attributable to the procedure.

The main advantage of this setup is the shorter (10 min) examination time. The 3T state-of-the-art scanner gives us an opportunity to perform high resolution morphologic work-up in a reasonable time. Furthermore, the ability to perform more sophisticated techniques preoperatively has now become a reality.

Case 1

A 67-year-old female patient was admitted due to seizure. Immediate preoperative MRI and functional MRI (left hand finger tapping paradigm) showed that there was a mass in the right frontal lobe including the eloquent motor cortex (Figs. 1A and B). Intraoperative MRI with the body coil demonstrated complete resection (Figs. 2A, B and C). One day later the follow-up examination confirmed the completeness of resection (Figs. 3A and B). Fiber tractography showed that there was no difference between preoperative (Figs. 4A and B) and postoperative (Figs. 5A and B) corticospinal tracts. Pathological exam revealed the mass as anaplastic astrocytoma. 6 months later, the patient was able to walk without assistance.

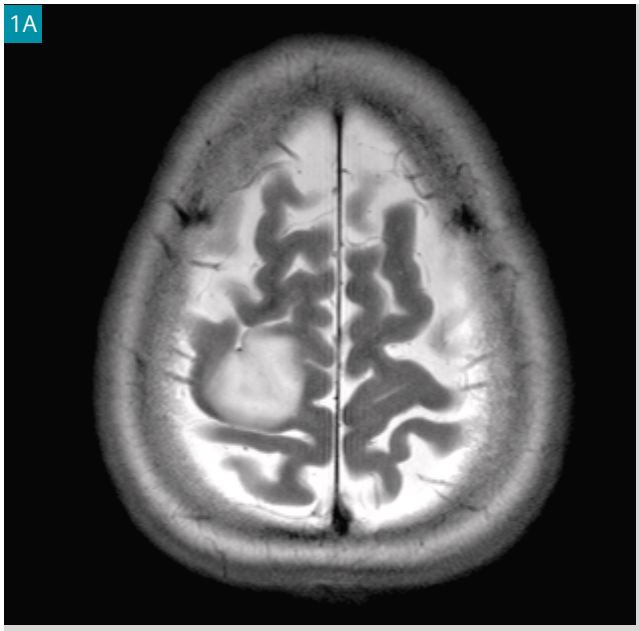

[Figure 1A] *Axial TSE T2-weighted (T2W) image.*

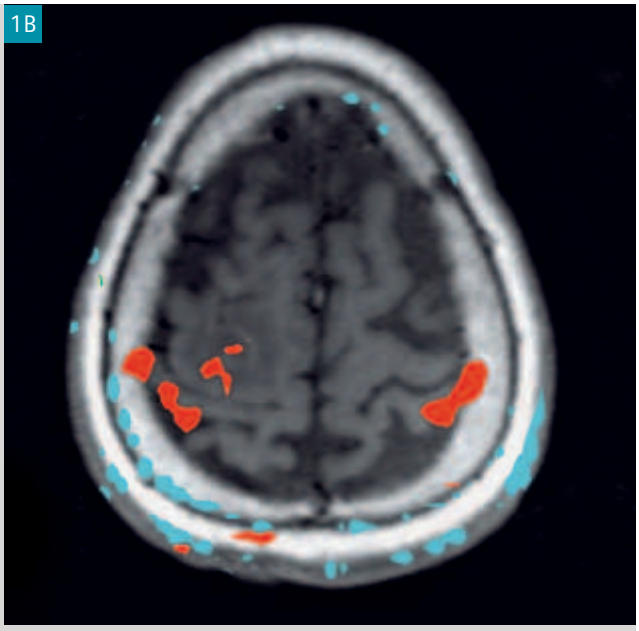

[Figure 1B] *Color coded parametric map.*

[Figure 2A] *Axial TSE T2W image.*

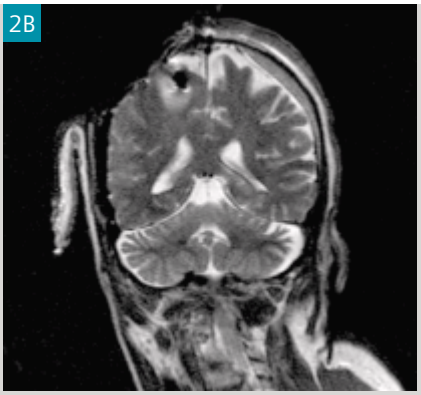

[Figure 2B] *Coronal TSE T2W image.*

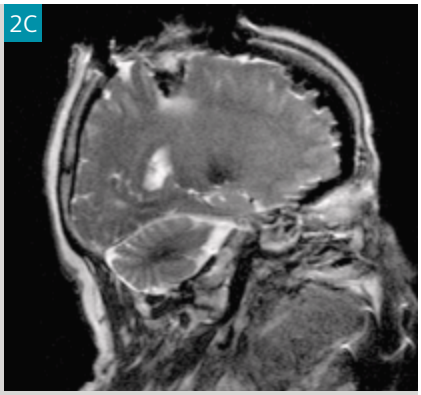

[Figure 2C] *Sagittal TSE T2W image.*

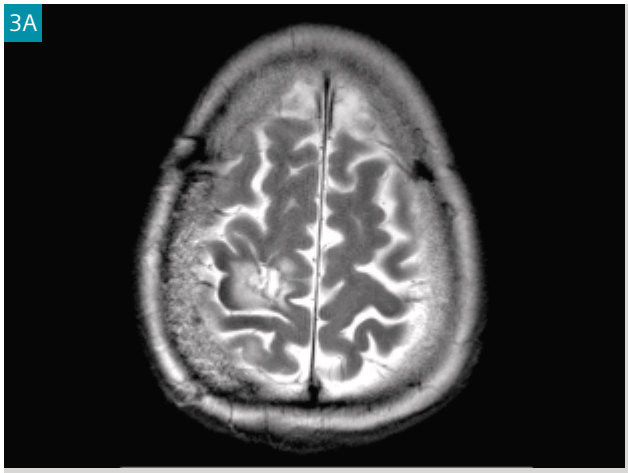

[Figure 3A] *Axial TSE T2W image.*

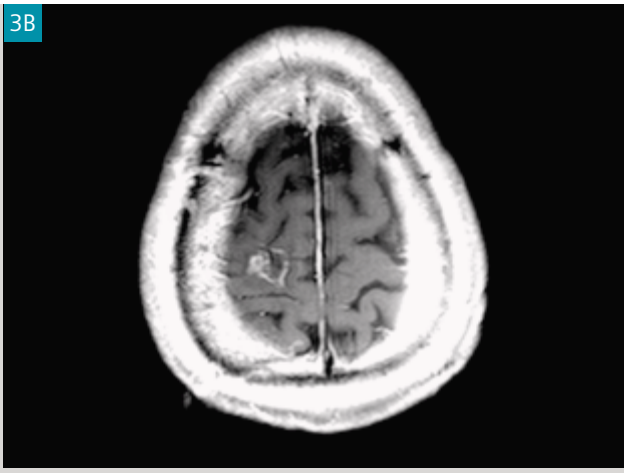

[Figure 3B] *Axial SE T1W image without contrast.*

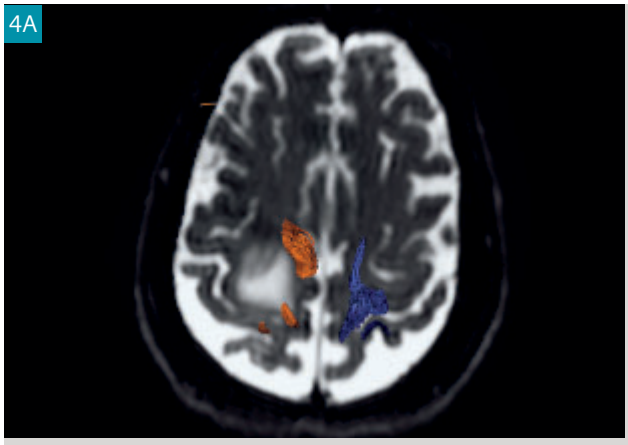

[Figure 4A] *Pre-operative DTI.*

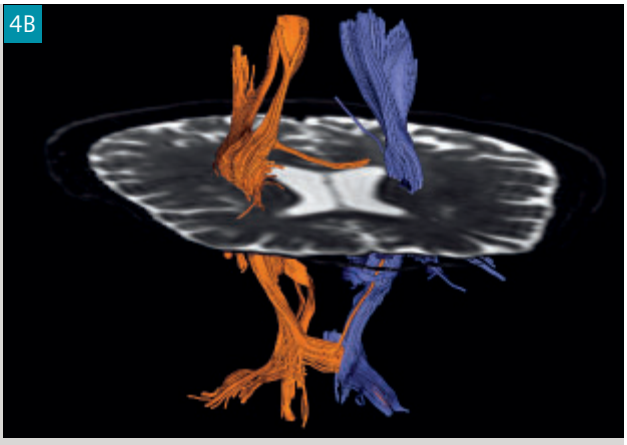

[Figure 4B] *Pre-operative DTI showing cortico spinal tracts.*

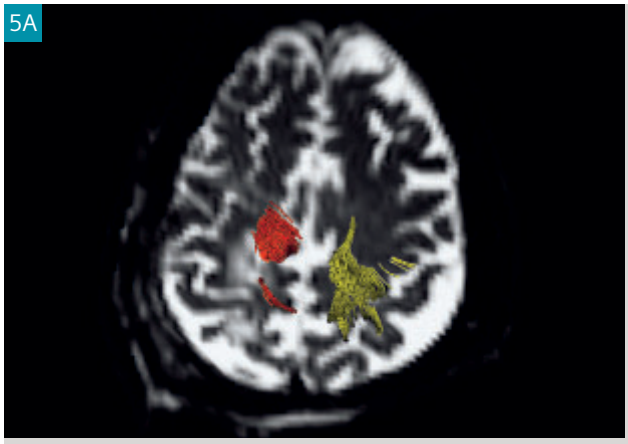

[Figure 5A] *Post-operative DTI.*

[Figure 5B] *Post-operative DTI showing corticospinal tracts showed no difference to the pre-operative ones.*

Case 2

A 70-year-old male had had 3 operations in another center due to non-functional macroadenoma of the pituitary gland. Follow-up MR examination carried out at another center revealed recurrence (Figs. 6A and B). During the operation the MR examination with the 8-channel head-coil (Figs. 7A and B) showed residual tumor in the suprasellar cistern near the stalk. The neurosurgeon decided to continue operating. A 24-hour follow-up exam demonstrated total resection (Figs. 8A and B).

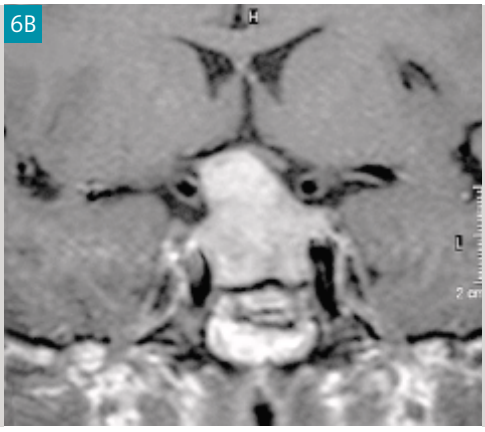

[Figure 6A]
Sagittal SE T1W with contrast

[Figure 6B]
Coronal SE T1W image with contrast

[Figure 7A]
Coronal TSE T2

[Figure 7B]
Sagittal TSE T2W image

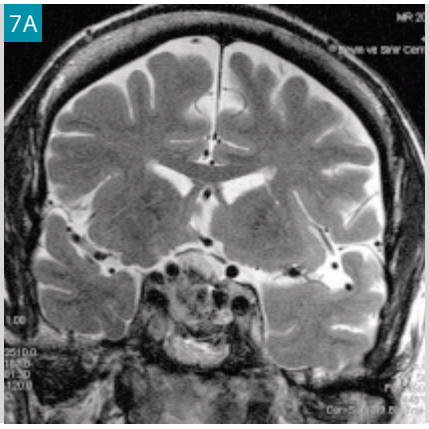

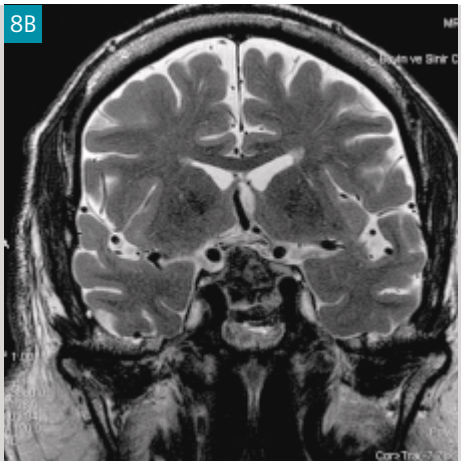

[Figure 8A]
Sagittal TSE T2W image

[Figure 8B]
Coronal TSE T2 image

Case 3

A 37-year-old male was admitted to the hospital due to seizure. He had undergone an operation 3 years previously for low grade astrocytoma of the left temporal lobe. After control MRI (Figs. 9A and B), which had revealed recurrent left temporal mass, the patient was operated on. Intraoperative MR (Fig. 10) showed incomplete resection of the tumor: the neurosurgeon decided to continue the operation. The imaging after further resection showed no residual tumor. (Fig. 11). Postoperative 24-hour follow-up examination with contrast also confirmed total resection of the tumor (Fig. 12).

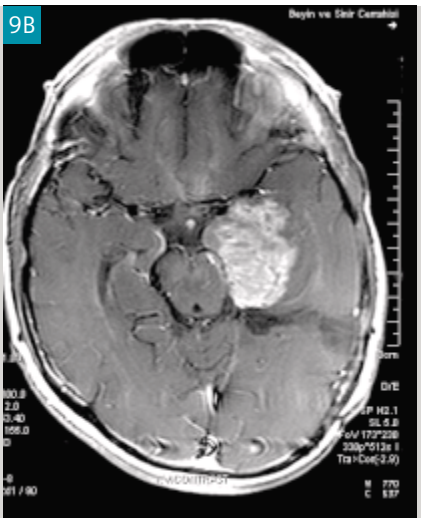

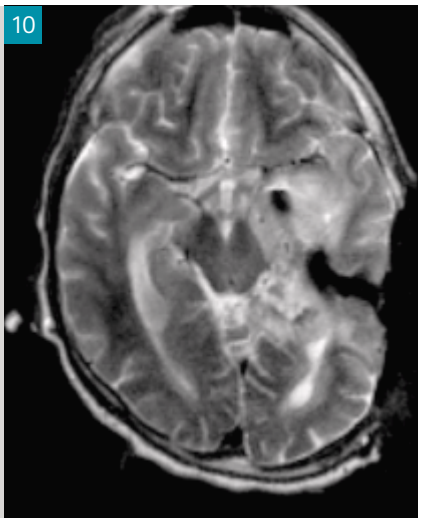

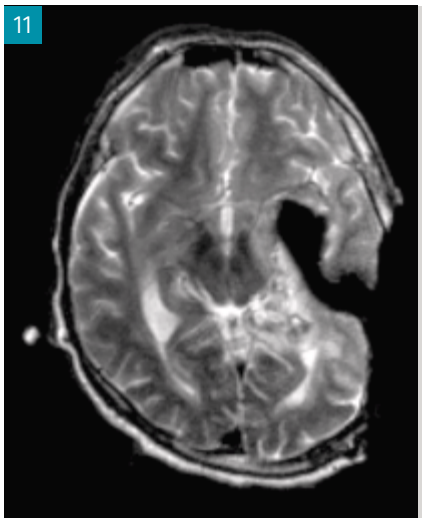

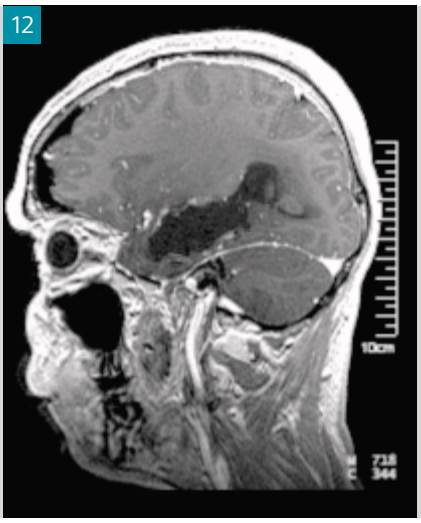

[Figure 9A] *Axial T2W image*

[Figure 9B] *Axial T1W image with contrast*

[Figure 10] *Axial T2W Image*

[Figure 11] *Axial T2W image*

[Figure 12] *Sagittal 3D MP-RAGE with contrast*

References

[1] Fenchel S, Boll DT, Lewin JS. Intraoperative MR imaging. Magn Reson Imaging Clin N Am 2003;11: 431–447.

[2] Nimsky C, Gansland O, Hastreiter P, Wang R, Benner T,Sorensen AG, Fahlbusch R. Preoperative and intraoperative diffusion tensor imaging-based fiber tracking in glioma surgery. Neurosurgery 2004; 56: 130–138.

[3] Nimsky C, Gansland O, Fahlbusch R. Comparing 0.2 Tesla Intraoperative With 1.5 Tesla Intraoperative Magnetic Resonance Imaging: Analysis of setup, Workflow, and Efficiency. Acad Radiol 2005; 12: 1065–1079.

Iron-Oxide Enhanced Susceptibility-Weighted Imaging of Lymph Node Metastasis

Ravi Seethamraju, Ph.D.[1], Milind Dhamankar, M.D.[1], Mukesh Harisinghani, M.D.[2]

[1]*Siemens Medical Solutions, Malvern, PA, USA*
[2]*Massachusetts General Hospital, Boston, MA, USA*

Introduction

Detection of local and regional lymph node metastases is important for determining therapy and prognosis in patients with various primary malignancies. Currently cross sectional imaging modalities like contrast enhanced* CT and MRI rely solely on size criterion as the primary yardstick for detection of malignant lymph nodes. However nodal size is not an accurate method, as not all malignant nodes are enlarged and conversely not all large nodes are malignant [1]. Thus a more robust and accurate technique is needed for staging lymph nodes which characterizes lymph nodes independent of their size. MRI enhancement with ultra-small super-paramagnetic iron oxide particle (USPIO) has shown to be an accurate and reliable imaging technique for detection of minimal nodal metastatic disease independent of lymph node size.

Commercial preparation of USPIOs like Ferumoxtran-10 (Combidex [Advanced Magnetics, Cambridge, Mass]; also known as Sinerem, AMI-7227, AMI-227, and BMS 180549) target the reticulo-endothelial system and have been specifically developed for MR lymphangiography. These agents are composed of an iron oxide crystalline core of 4.3–6.0 nm covered by low-molecular-weight dextran. Their T1 and T2 relaxations are 2.3 x 10^4 and 5.3 x 10^4 mol^{-1} sec^{-1} (20 MHz, 39°C), respectively, in 0.5% agar.

Upon intravenous injection, these contrast agents are transported to the lymph nodes binding to specific receptors within the nodal macrophages. If the lymph nodes are benign, the macrophages function normally and phagocytose the intravenously administered nanoparticles. Thus normal lymph nodes show a drop in signal intensity on MRI imaging after Ferumoxtran-10 administration due to the susceptibly from phagocytosed nanoparticles. In contrast, malignant infiltration results in lack of macrophages and hence these regions, due to the lack of iron oxide uptake, retain their high signal intensity. This is the underlying principle behind MR lymphangiography.

Imaging

Metastasis in normal-sized lymph nodes can be of the order of 4–9 mm [2], hence from the MR viewpoint it is very essential that the maximum voxel dimension should not exceed 2 mm for capturing even the least amount of metastasis in a lymph node. While this restriction was routine in the case of in-plane dimensions, through-plane dimensions were restricted in the case of multi-echo gradient echo (MEGE) sequences. MEGE sequences are very essential for MR lymphangiography as they facilitate the computation of T2* which is an indicator of malignancy. This problem has been alleviated with the development of the new works in progress T2*-weighted Multi-Contrast Gradient Echo (MCGE) sequence at Siemens Medical Solutions.

The Sequence

Currently the MCGE sequence supports a maximum of 12 contrasts with the facility to choose a bi-polar or mono-polar readout. While bi-polar readouts are standard for Gradient Echo sequences, they suffer from chemical shift artifacts that shift between echoes. This essentially destroys any in-plane resolution advantage as they tend to spoil the computation of T2* in the regions that are chemically shifted. The mono-polar readout, however, maintains the chemical shift by using a gradient rewinder between readouts so that all the k-space lines are acquired in the same direction. The availability of integrated Parallel Acquisition Techniques (iPAT) in these sequences further saves acquisition time.

The Protocol

Currently the protocol has been optimized for pelvic studies and has been successfully tested on patients. Apart from the MCGE sequence, a VIBE and T2-weighted spin echo sequences are used for obtaining spatial and anatomical characterization of the nodes. The protocol is applied twice, once before the administration of the contrast agent and 24 hours after the administration of the contrast agent. The individual compo-

nents of the protocol as currently tested on a 1.5T MAGNETOM Avanto are as follows:

1. A T1-weighted (T1W) 3D VIBE non breath-hold sequence with TE 1.9 ms, Flip Angle = 12°, TR 5 ms, BW 260 Hz/Px, FOV 340 x 340 mm and 1.3 x 1.3 mm and interpolated slice thickness of 2.68 mm acquired coronally to cover around 100 slices acquired in 2 minutes. These images are required for a MIP of the vasculature that will serve as a reference for location of the nodes.
2. A T2-weighted TSE non breath-hold sequence with TE 76 ms, Flip Angle 90°, TR 4000 ms, BW 160 Hz/Px, FOV 340 x 340 mm and slice thickness of 2.68 mm acquired axially to cover around 30 slices acquired in roughly 3 minutes. Though the T2-weighted images are not preferred for quantification of the metastasis, they are excellent in terms of signal-to-noise ratio (SNR) and devoid of blooming artifacts resulting from the susceptibility of iron, so node delineation and identification is easier on these images.
3. The T2*-weighted MCGE non breath-hold sequence with TE 8.8 ms to 70 ms (12 contrasts), Flip Angle 75°, TR 1800 ms, BW 130 Hz/Px, FOV 214 x 380 mm and slice thickness of 2 mm acquired axially to cover 45 slices in 6 minutes with iPAT factor of 2. All sequences use a 0 mm gap between slices.

Initial Experiences

After initially experimenting on an oil-water phantom, the protocol was tried on a patient. The T2* MCGE sequence was also run in the bi-polar mode for comparison. In the case of bi-polar mode the acquisition time was reduced roughly by a factor of two due to the absence of the rewinder between echoes. The images from the first echo and the corresponding T2* computed from the echoes are presented in Fig. 1. It can be seen very clearly that for the same echo time and windowing that the image from the monopolar sequence is crisper and hence the computed T2* is more reliable.

Fig. 2 shows pre- and post-contrast T2-weighted images. Note how the node is easy to discern, especially the partial fatty infiltration. Fig. 3 is a VRT rendering of the vasculature

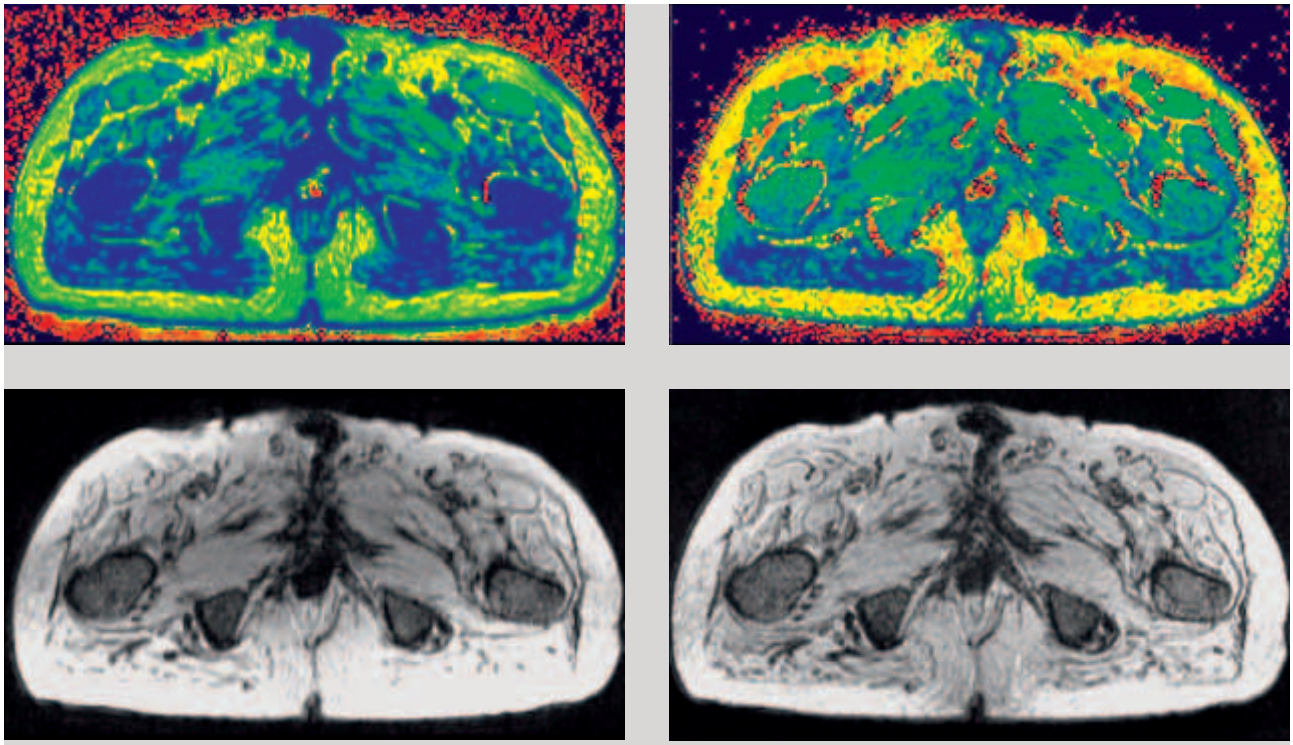

[Figure 1] *Comparison between bi-polar and mono-polar images. Images in top row are T2* maps and bottom row are single echo images at same echo time. Images on the left are from the bi-polar sequence and on the right are from the mono-polar sequence. Note how the images from the mono-polar sequence have more detail than those from the bi-polar sequence. This is due to the averaging effect of the alternating phase shifts in the bi-polar sequence.*

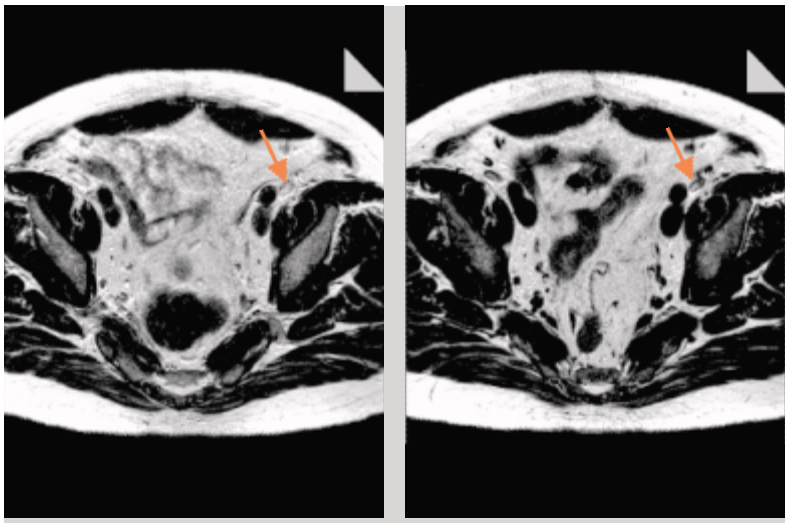

[Figure 2] *T2-weighted TSE axial slice showing partial fatty infiltration in the node. The image on the left is pre-contrast and on the right is post-contrast. Note that on the post-contrast image a portion of the node still remains bright while the rest of the node has become very dark. This is because the USPIO is not absorbed by the fatty infiltration. To differentiate fatty infiltration from metastases, the shape of the lymph node and the hypo intensity need to be taken into account. A fat suppressed T1 can also give clues on the fatty infiltration.*

[Figure 3] *Segmented nodes color coded on a VRT rendered vasculature. Information from segmented nodes is coded with unique values that are then combined with information from the T1-weighted 3D VIBE images to obtain the VRT rendering of the nodes on the vasculature. Benign nodes are coded green and malignant red.*

with segmented nodal information from the T2 images superimposed with color coded information from the T2*s. This has been achieved by the use of a works in progress *syngo* task card that has been optimized for the workflow of the current protocol.

Conclusion

With the usage of a mono-polar multi-contrast GRE sequence it has been demonstrated that the estimation of T2* is vastly improved, thereby improving the detection of metastatic lymph nodes.

Future Directions

With Tim (Total imaging matrix) technology, it is now possible to flexibly combine coils to increase the field of view for metastatic evaluation beyond a localized region.

Implementation on 3T would offer interesting insights and challenges. While there will be an improvement in SNR and reduction in acquisition time, susceptibility artifacts will be more pronounced.

Optimization with respect to echo times and number of echoes is in progress. Reduction in number of echoes without any increase in noise would greatly help reduce the acquisition time, since with breath-holding in the case of abdominal studies time will be a factor. Addition of navigators on the other hand would also help in the case of abdominal studies.

Acknowledgements

We wish to acknowledge John Kirsch of Siemens Medical Solutions whose expert advice was crucial to the optimization of the protocols.

* This information about this product is preliminary. The product is under development and not commercially available in the US, and its future availability cannot be ensured.

References

[1] Harisinghani M.G., Weissleder R., Sensitive, Noninvasive Detection of Lymph Node Metastases, PLOS 2004, Vol. 1., (3): 202–209.

[2] Deserno W.M.L.L.G., Harisinghani M.G., et. Al., Urinary Bladder Cancer: Preoperative Nodal Staging with Ferumoxtran-10 enhanced MR Imaging, Radiology 2004; 233: 449–456.

Intravenous Cellular MR Contrast Agent* with a Great Clinical Potential

Jelle Barentsz, M.D., Ph.D.

Department of Radiology, UMCN, Nijmegen, The Netherlands

Introduction

Pelvic lymph node metastases have a significant impact on the prognosis of patients with malignancies. In prostate cancer, for example, even micro metastases in a single node rule out surgical cure by the available treatment protocols. For bladder cancer lymph node metastases are also significant. More than 5 lymph node metastases or extra capsular growth precludes curative surgical treatment. Thus, the status of the lymph nodes largely dictates the management of the primary tumour.

Surgical open pelvic lymph node dissection (PLND), considered to be the only reliable method for assessing lymph node status, is an invasive procedure associated with potential complications and side effects. A noninvasive, reliable method for detecting and staging nodal metastasis would reduce unnecessary surgery. Routine cross-sectional imaging modalities like CT and MRI lack the desired sensitivity in identifying metastases as they largely rely on size criteria only, and small metastases in normal size nodes can be missed. Moreover, differences in signal intensity on MR images between normal and cancerous nodes as well as gadolinium enhancement have also proven to be unreliable. Although very promising in metastatic lung cancer, the role of ^{18}FDG PET-scanning is limited in the urinary tract region, as ^{18}Fluorodeoxyglucose accumulates in the urinary bladder and kidneys. This makes an evaluation of metastases at this site difficult. Also in various tumors like prostate and bladder cancer this method is further limited by its low uptake in metastatic nodes. Although the sensitivity of ^{18}FDG PET is

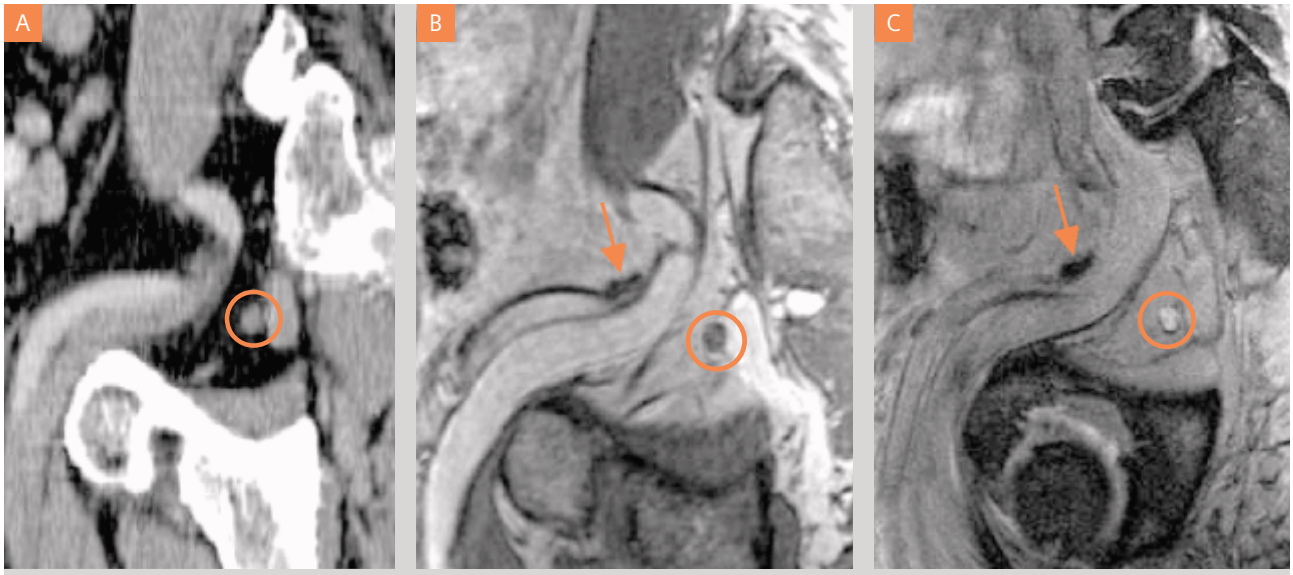

[Figure 1] ***Normal node and small positive node in 60-year-old male with prostate cancer.*** [A] *CT scan in semi-sagittal plane shows normal size (6 mm) node (circle).* [B] *Post ferumoxtran-10 T1-weighted TSE MR image (which is insensitive to iron) shows 2 grey normal size nodes (circle, arrow).* [C] *On post ferumoxtran-10 T2*-weighted MEDIC MR image (which is iron sensitive) one node is black (arrow) and the other one is white (circle). On histopathology the black node was normal and the white one was metastatic.*

slightly better (67%) compared to those of CT and unenhanced MR imaging, this value is, however, not high enough to replace pelvic lymph node dissection.

Ultra small super paramagnetic iron oxide particles (ferumoxtran-10) with a long plasma circulation time have been shown to be suitable as an MR contrast agent for intravenous MR lymphangiography [1, 2]. After IV injection, the ferumoxtran-10 particles are taken up by macrophages are transported to the interstitial space and from there through the lymph vessels to the lymph nodes (Figure 2). Thus this contrast agent is cell specific (for macrophages). Once within normally functioning nodes, the intracellular ferumoxtran-10 within the macrophages reduces the signal intensity of normal node tissue, because of the T1 and T2*- susceptibility effect of iron oxide, thus producing a signal drop or negative enhancement. In areas of lymph nodes that are involved with malignant cells, macrophages are replaced by cancer cells. Therefore, there is in these areas no uptake of the ferumoxtran-10 particles. In addition, due to increased vascular permeability and increased diffusion in cancer tissue, there is minimal leakage of ferumoxtran-10 particles into the extra cellular space of malignant metastatic areas, which produces a low local concentration and non-clustering of ferumoxtran-10 particles at these sites [3]. Through their T1-relaxivity this can induce an increase in signal intensity on T1-weighted images, producing positive enhancement [4]. Thus the ability of post ferumoxtran-10 MRI exams to identify metastatic areas in the lymph nodes depends primarily on the degree of uptake of ferumoxtran-10 by the macrophages in normal lymph node tissue and the leakage of ferumoxtran-10 particles in the metastatic area itself. Twenty-four hours after intravenous injection of ferumoxtran-10 normal lymph node and malignant tissue have different signal intensity on MR images. Therefore, this non-invasive technique may result in the detection of metastatic deposits in normal-size nodes (Figure 1).

Optimal evaluation of post ferumoxtran-10 images should be done by comparing pre- with post-contrast MR images in the same plane. On the pre-contrast images the shape, the size, and the location of the nodes can be assessed. On the post-contrast MRI the signal intensity change can be evaluated. However, this requires two MRI examinations, which limits this technique. This problem can be solved by only performing a post-ferumoxtran-10 MR exam, using both a sequence which is insensitive for iron such as a T1- or proton weighted TSE sequence, and a sequence which is sensitive to iron. For the latter purpose a good sequence is a high resolution T2*-weighted MEDIC (TE ~18 ms). The T1/PW TSE sequences yield high resolution images without (susceptibility) artifacts, whereas the T2*-sequence gives information about the iron content of the nodes. It is, therefore, important to apply both sequences with the same resolution and slice positioning parameters. In pelvic tumors (prostate cancer), this can be best done in a plane parallel to the psoas muscles (obturator, or semi-sagittal plane, Figure 1), and the axial plane, covering the para-aortic until the femoral region (Figure 3). In the "reading" of the images, a one-by-one comparison gives the best results (Figure 1). Incidentally in this way even a 2 mm metastatic node can be found (Figure 3).

Uptake mechanism of ferumoxtran-10

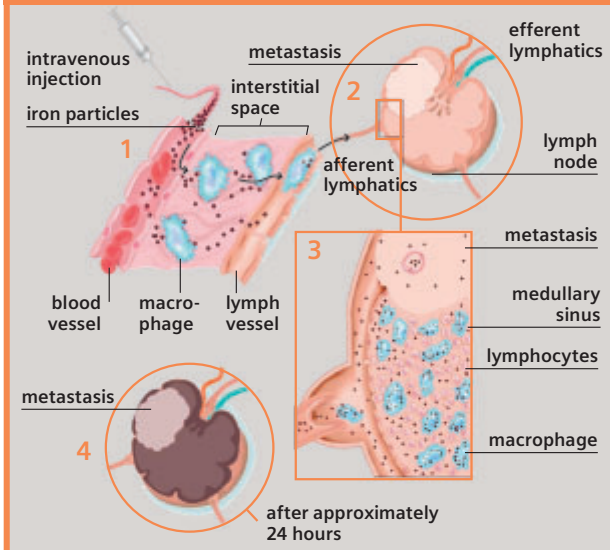

[Figure 2] *IV injected particles slowly extravasate from vascular to interstitial space (1) and then are transported to lymph nodes via lymphatic vessels (2). In lymph nodes, particles are internalized by macrophages (3), and these intracellular iron-containing particles cause normal nodal tissue to have low signal intensity. Disturbances of lymph flow or nodal architecture by metastases lead to abnormal accumulation patterns depicted by the lack of decreased signal intensity (4).*
Reprinted with permission of authors from Radiology.[6]

Clinical value

When using high resolution MR-technique small metastases can be prospectively recognized in small (3–10 mm) size lymph nodes [5]. These small lymph nodes would be considered to be benign in plain MRI or CT examinations. In addition, hyperplastic enlarged nodes can be correctly recognized as non metastatic, based on their low signal intensity. This results in improved sensitivity (~ 90%), with remaining

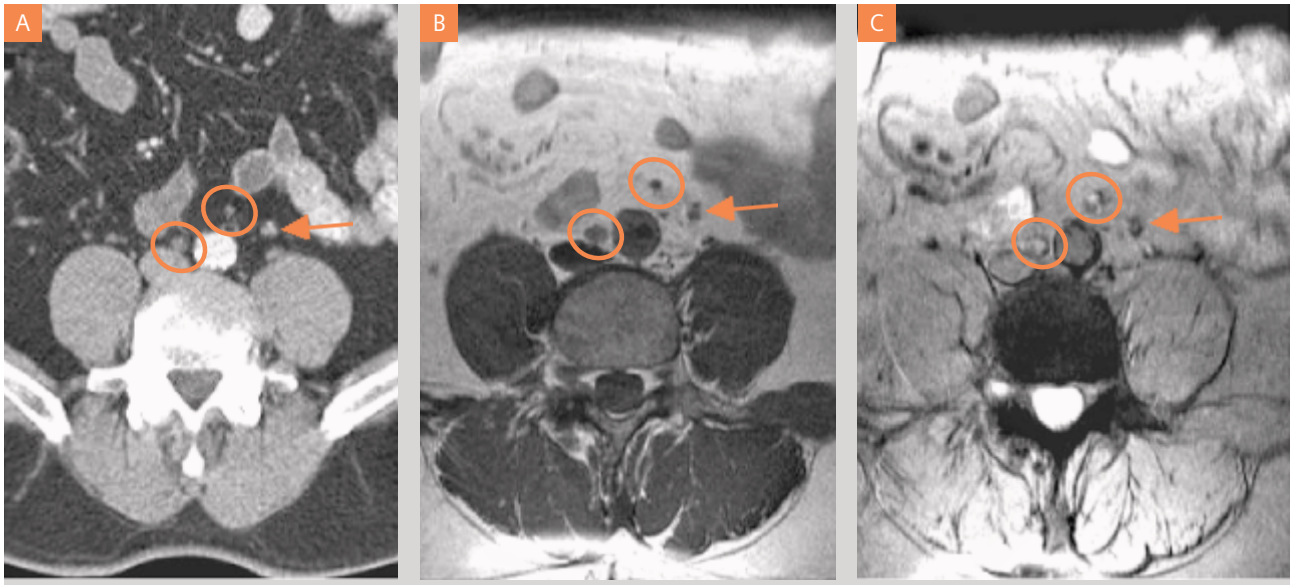

[Figure 3] *58-year-old patient treated for prostate cancer with nodal recurrence. CT and MRI obtained 2 years after lymphadenectomy, prostatectomy and hormonal therapy. Now PSA increased from 0 to 1.8.* [A] *CT scan in axial plane shows 3 normal size node (circle right 5 mm; circle left 2 mm).* [B] *Post ferumoxtran-10 T1-weighted TSE MR image (which is insensitive to iron) shows the same 3 grey nodes (circles, arrow).* [C] *On post ferumoxtran-10 T2*-weighted MEDIC MR image (which is iron sensitive) one node is black (arrow) and the other 2 are white (circles). On histopathology the black node was normal and the whites were metastatic.*

equal high specificity (~ 95%) in various tumors (Figure 4) [5–8]. In prostate cancer, contrast-enhanced CT and conventional MRI have a low sensitivity (40%), which is improved to 100% on a patient level and to 90% on a nodal level [5].

In urinary bladder cancer, 10/12 metastatic normal size lymph nodes were detected with ferumoxtran-10 MRI only. This resulted in an improved sensitivity (from 76% to 96%), whereas the specificity did not change significantly (from 99% to 95%) [6]. When using ferumoxtran-10 MRI, patients may be reliably selected for cystectomy, prostatectomy or radiotherapy without the need for invasive and costly procedures such as open and laparoscopic PLND. Furthermore, if the node is > 5 mm the presence of malignancy can be confirmed by image guided biopsy, and thus also avoid PLND in these patients. This was the case in 5/80 (6%) patients in the study of Harisinghani and Barentsz. All 5 nodes were confirmed positive. Finally, with ferumoxtran-10 MRI all pelvic nodes are visualized. Harisinghani and Barentsz showed that in 11% of their patients thanks to ferumoxtran-10 MRI metastatic nodes were detected, which were outside the classical field of lymph node resection [5]. In patients with a suspicion for a recurrence, e.g. in patients with a PSA-relapse after treatment, this technique may show metastatic nodes when they still are small (Figure 3), thus allowing earlier adequate therapy. Finally, identifying small pathologic nodes will facilitate more appropriate use of sophisticated radiation therapy. For example when positive nodes are accurately identified, precise intensity modulated radiotherapy can be performed. This results in an increased dose on the malignant nodes and a decreased dose, with reduced side-effects, on normal tissues.

In head and neck cancers, 25% lymph nodes are positive despite negative preoperative imaging (contrast CT and US biopsy) as metastatic nodes are small (5–10 mm). In addition PET is nonspecific and does not provide anatomic location. Therefore, extensive surgery -radical neck dissection- is performed in virtually all patients. This results in cosmetic deformity and a complication rate of 36-54%. Mack et al. reported that ferumoxtran-10 MRI was accurate in 26/27 (96%) patients, which resulted in reduction in surgery by 26% of patients [7]. Early results with ferumoxtran-10 MRI scans in breast cancer show a sensitivity of 78%, a specificity of 96% and a negative predictive value of 97% (Figure 5) [8]. The sentinel lymph node procedure in breast cancer has a 3% to 10% false negative rate. Furthermore, positive internal mammary lymph nodes are missed in 17% of cases. Finally, the sentinel lymph node is the only positive node in 61% lymph node positive patients.

These patients all undergo axillary dissection, with a subsequently high rate of clinically significant lymph edema. Thanks to its high negative predictive value, potentially in patients with a negative ferumoxtran-10 MRI, the axillary dissection may be avoided. Further studies are underway to validate this statement.

Finally, we believe that novel 3D reconstruction techniques would be of particular help in displaying and analyzing the massive amount of high resolution data. In this sense it should be feasible to display both normal and abnormal lymph nodes and their location with respect to important surgical landmarks like vessels, obturator nerves and ureters in 3D.

Summary

The combination of a macrophage (= cell) specific MR-contrast agent and high resolution MR imaging allows the detection of small and otherwise undetectable lymph node metastases in patients with pelvic cancer. This has an important clinical impact, as the diagnosis will be more precise and can be obtained in a less invasive maner. Subsequently this will reduce morbidity and healthcare costs. However, thorough knowledge of sequence parameters and planes, lymph node anatomy, appearance of normal and abnormal nodes, and pitfalls is essential when using this technique. This implies a very important role for education by expert radiologists, MR-manufacturers, and contrast agent companies.

**This article discusses clinical uses which are not commercially available in the US.*

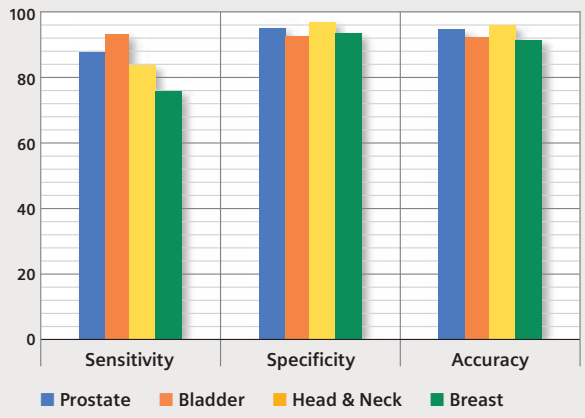

[Figure 4] *Results of ferumoxtran-10 of various tumors [5–8].*

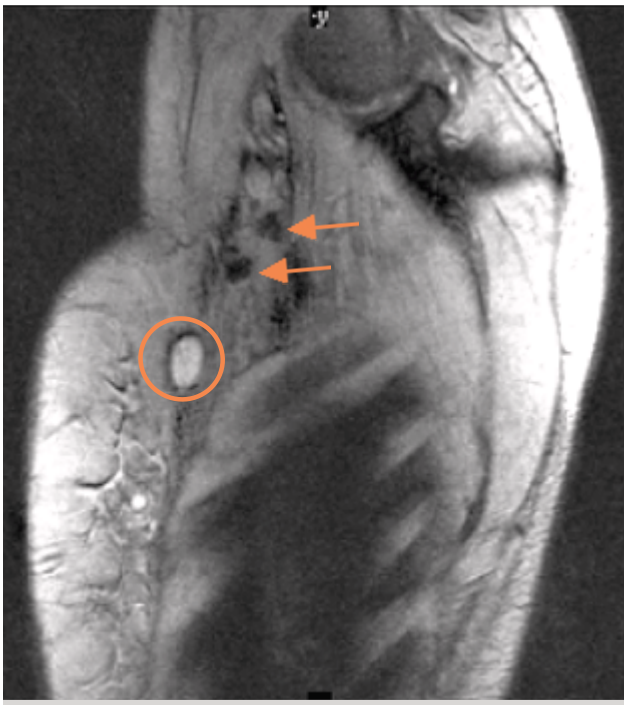

[Figure 5] ***55-year-old patient with breast cancer and positive lymph node.*** *Sagittal post ferumoxtran-10 T2*-weighted MEDIC MR image shows one white (circle) and 2 dark nodes (arrows). The white node showed on histopathology metastases, the dark ones were normal.*

References

[1] Vassallo P, Matei C, Heston WDW, et al. AMI-227-enhanced MR Lymphography: usefulness for differentiating reactive from tumor bearing lymph nodes. Radiology 1994; 193: 501–506.

[2] Weissleder R, Elizondo G, Wittenberg J et al. Ultrasmall paramagnetic iron oxide: an intravenous contrast agent for assessing lymph nodes with MR imaging. Radiology 1990; 175: 494–498.

[3] Gerlowski LE, Jain RK. Microvascular permeability of normal and neoplastic tissues. Microvasc. Res. 1986; 31: 288–305.

[4] Bellin MF, Roy C, Kinkel K, Thoumas D, Zaim D et al. Lymph node metastases: safety and effectiveness of MRI with Ultrasmall Superparamanetic Iron Oxide Particles. Initial clinical experience. Radiology 1998; 207: 799–808.

[5] Harisinghani M & Barentsz J, Hahn P, Deserno W, et al. Noninvasive detection of clinically occult lymph-node metastases in prostate cancer. NEJM 2003; 348: 2491–2499.

[6] Deserno WM, Harisinghani MG, Taupitz M, Jager GJ, Witjes JA, Mulders PF, Hulsbergen van de Kaa CA, Kaufmann D, Barentsz JO. Urinary bladder cancer: preoperative nodal staging with ferumoxtran-10-enhanced MR imaging. Radiology 2004; 233: 449–56.

[7] Mack MG, Balzer JO, Straub R, Eichler K, Vogl TJ. Superparamagnetic Iron Oxide-enhanced MR Imaging of Head and Neck Lymph Nodes. Radiology 2002; 222: 239–244.

[8] Michel SCA, Keller TM, Fröhlich JM, Fink D, Caduff R, Seifert B, Marincek B, Kubik-Huch R. Preoperative Breast Cancer Staging: MR Imaging of the Axilla with Ultrasmall Superparamagnetic Iron Oxide Enhancement. Radiology 2002; 225: 527–536.

Hold the date for the MAGNETOM World Meeting at ISMRM 2006 Seattle, Washington, USA

Monday, May 8th, 7:30 p.m. – 11:00 p.m., Benaroya Hall, 200 University Street, Seattle

Now you can get the latest information about hot topics in MRI at the Benaroya Hall. Siemens invites the MAGNETOM World members to a memorable scientific information session. This meeting also offers the opportunity to join other MAGNETOM World members, share thoughts and exchange ideas with them.

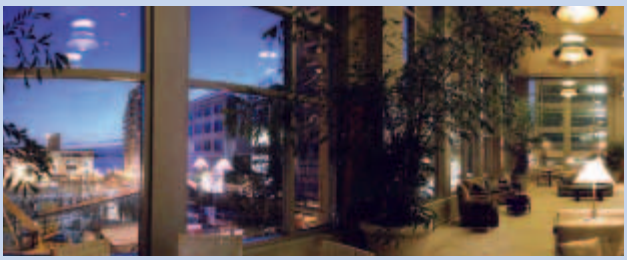

Benaroya Hall lies in the heart of downtown Seattle. It occupies the entire block between 2nd & 3rd Avenues, and Union & University Streets. The public entrance to the Hall is along 3rd Avenue.

All attendees must register prior to April 24th at
➔ **http://siemens.remoteevent.com/ISMRM2006**